The habenula clock influences prediction of danger

Adriana Basnakova[1, 2], Ruey-Kuang Cheng[3], Joanne Chia Shu Ming[3], Giuseppe D'Agostino[3], Suryadi[4], Germaine Tan Jia Hui[3], Sarah R. Langley[3] and *Suresh Jesuthasan[2, 3]

[1]School of Biological Sciences, University of Manchester, UK.
[2]Institute of Molecular and Cell Biology, Singapore.
[3]Lee Kong Chian School of Medicine, Nanyang Technological University, 59 Nanyang Drive, Singapore 636921.
[4]School of Physical and Mathematical Sciences, Nanyang Technological University Singapore.
*corresponding author: sureshj@ntu.edu.sg

Abstract

The response of an animal to a sensory stimulus depends on the nature of the stimulus and on predictions mediated by spontaneous activity in neurons. Here, we ask how circadian variation in the prediction of danger, and thus the response to a potential threat, is controlled. We focus on the habenula, a mediator of threat response that functions by regulating neuromodulator release, and use zebrafish as the experimental system. Single cell transcriptomics indicates that multiple clock genes are expressed throughout the habenula, while quantitative in situ hybridization confirms that the clock oscillates. Two-photon calcium imaging indicates a circadian change in spontaneous activity of habenula neurons. To assess the role of this clock, a truncated *clocka* gene was specifically expressed in the habenula. This partially inhibited the clock, as shown by changes in *per3* expression as well as altered day-night variation in dopamine, serotonin and acetylcholine levels. Behaviourally, anxiety-like responses evoked by an alarm pheromone were reduced. Circadian effects of the pheromone were disrupted, such that responses in the day resembled those at night. Behaviours that are regulated by the pineal clock and not triggered by stressors were unaffected. These findings establish that the habenula clock regulates the expectation of danger, thus identifying one mechanism for circadian change in the response to a stressor.

Keywords: anxiety, circadian clock, habenula, spontaneous activity, predictive coding.

1. Introduction

Expectations play a major role in determining the response of a person or animal to a sensory stimulus or situation. In this framework, known as predictive coding, the brain is not a passive recipient of stimuli, but actively generates predictions that are updated by experience (Barrett, 2017; Friston, 2018). Thus, encountering a cue such as the smell or sound of a predator increases the expectation of danger, turning a normally innocuous stimulus into a threat. Abnormal expectations, or predictions, have been proposed to underlie stress-related conditions such as post-traumatic stress disorder. Predictions are mediated by spontaneous activity in the brain (Berkes et al., 2011), while updating of expectations is enabled by the release of neuromodulators. Dopamine and serotonin contribute to the comparison of current input with pre-existing expectations. When outcomes surpass predictions, dopamine release by neurons in the midbrain increases; when there is disappointment, dopamine release is

inhibited (Schultz, 1998). Serotonin release by the raphe provides an indication of the magnitude of the prediction error (Matias et al., 2017). Acetylcholine appears to have a role in setting the precision of predictions (Moran et al., 2013). Behaviour and emotional states can thus be understood to be the result of genetically encoded programs that are continuously modified by predictions, enabling the animal to respond optimally to perceived reality.

The habenula, which contains several subdomains, has emerged in recent years as an important regulator of several neuromodulators involved in predictive coding. The medial habenula in zebrafish (Hong et al., 2013), like that of mouse (Ren et al., 2011), includes cholinergic neurons. Disruption of specific subdomains of the medial habenula leads to anxiety-like behaviour (Agetsuma et al., 2010; Lee et al., 2010) or aversion (Hsu et al., 2014) that is experience dependent. The lateral habenula regulates midbrain dopaminergic and serotonergic neurons, and phasic activity occurs here when there is an unexpected punishment or absence of reward (Matsumoto and Hikosaka, 2009). As an animal learns the actions that prevent punishment, this activity lessens (Amo et al., 2014). In addition to activity that is evoked by sensory stimuli or perceptions of reward, the habenula displays spontaneous activity (Jetti et al., 2014; Kim and Chang, 2005). Excessive levels of burst firing, which can be interpreted as constant negative prediction, has been detected in the lateral habenula of animals with depressive behavior (Andalman et al., 2019; Yang et al., 2018). To understand how mood and behaviour are shaped, it is thus important to not only understand how the habenula responds to reward and sensory input, but to also investigate how spontaneous activity is regulated.

One factor that affects the level of spontaneous activity in neurons is the molecular clock. The molecular clock in most organisms consists of a transcriptional-translational feedback loop with a period of ~ 24 hours (Takahashi, 2017). Core components of the clock in animals include heterodimers of Clock and Arntl (Bmal), which enter the nucleus in the daytime. Here, they drive transcription of *period* (*per*) and *cryptochrome* (*cry*) genes, which then inhibit the Clock-Arntl heterodimer. Clock and Arntl also control transcription of channels that affect resting membrane potential in neurons, driving this close to threshold and thus increasing spontaneous firing rate in the daytime (Harvey et al., 2020). Components of the clock machinery are found in nearly all cells, including those of the habenula (Baño-Otálora and Piggins, 2017; Mendoza, 2017), and the habenula molecular clock continues cycling for

multiple days even in the absence of the main pacemaker of the brain, the suprachiasmatic nucleus (Guilding et al., 2010; Salaberry et al., 2019). Spontaneous firing in the habenula of rat (Zhao and Rusak, 2005) and mouse (Guilding et al., 2010; Sakhi et al., 2014a, 2014b) varies across a circadian cycle, in both the lateral and medial habenula. The significance of the habenula clock is unclear, however. Given the role of habenula activity in predictive coding, we hypothesize that the clock causes a circadian change in behaviours that are modified by recent experience. To test this, we use the zebrafish as the experimental system. We examine anxiety-like behaviour, which is increased by expectation of danger.

2. Materials and Methods

2.1 Single cell data reanalysis

Count tables were downloaded from Gene Expression Omnibus, accession number GSE105115. All processing downstream was done using R/BioConductor (R 4.0.2/Bioconductor 3.12) packages designed to handle single cell data using the SingleCellExperiment class (v. 1.12.0) (Amezquita et al., 2020). A detailed explanation with code and figures is provided as a GitHub repository at https://github.com/langleylab/habenula_reanalysis. Briefly, gene-level count tables from the SmartSeq2 experiment were merged retaining the information on the plate of origin. Genes that were not detected in any barcode were removed. Barcodes were discarded according to the following criteria: low expression, low number of genes detected, high percentage of *malat1* expression, high percentage of mitochondrial transcripts expression and high percentage of ribosomal transcript expression. Thresholds for every criteria were set as 3 Mean Absolute Deviations (MADs), with the exception of mitochondrial % which was set at 4 MADs. Outlier calculations were done separately in each plate using the *isOutlier* (using the *batch* argument) and *perCellQCMetrics* functions from the *scater* package (v. 1.18.6) (McCarthy et al., 2017). These filters yielded 17673 genes and 1140 barcodes for downstream analyses. Barcodes were then clustered using the *quickCluster* function from the *scran* package (v. 1.18.5 (Lun et al., 2016)), blocking for the plate of origin. Per-cell size factors were then determined by deconvolution using *scran*, and they were used to perform multi-batch normalization (batching by plate) using the *multiBatchNorm* function from the *batchelor* package (v. 1.6.2 (Haghverdi et al., 2018)). Highly variable genes were estimated on the multi-batch normalized data blocking by plate using the *modelGeneVar* function from

114 the *scran* package, which estimates the mean-variance trend and decomposes variance for
115 each gene in technical and biological components according to the deviation from the trend.
116 Variances were combined across plates using the *combineVar* function from *scran*, and the
117 2000 genes with the highest biological variance were selected using the *getTopHVGs*
118 function from *scran*. These were used as an input to perform dimensionality reduction via
119 Principal Component Analysis as implemented in the *BiocSingular* package (v. 1.4.0, (Lun,
120 2020a)).
121
122 The first 50 principal components were then used as an input to perform batch (plate) effect
123 correction via the *fastMNN* function from *batchelor*, which determines a correction vector in
124 PCA space using mutual nearest neighbour pairs to estimate the amount and direction of
125 necessary correction. The dimensionality of the corrected space, i.e. the number of most
126 relevant dimensions for subsequent steps, was determined using the *maxLikGlobalDimEst*
127 function from the *intrinsicDimension* package (v. 1.2.0 (Johnsson et al., 2014)). The value for
128 the *k* parameter for this function (k = 30) was determined as the rounded square root of the
129 number of cells, and the estimation yielded 13 dimensions. Subsequently, the first 13
130 dimensions of the corrected space were used to run the t-stochastic neighbour embedding (t-
131 SNE) algorithm for data visualization, and to construct a Shared Nearest Neighbour (SNN)
132 graphs for clustering. Several SNN graphs were constructed at different resolutions, i.e. 10,
133 15, 30, 40 and 50 neighbours were considered for the graph construction; all edges were
134 weighted by the Jaccard similarity between the neighbours of each node. SNN graph
135 construction was performed using the *buildSNNGraph* function from *scran*. Then, the
136 Louvain community detection algorithm (as implemented in the *igraph* package (v. 1.2.6
137 (Csardi and Nepusz, 2006)) was used to identify clusters. Relationships between different
138 clustering results (obtained by using different neighbours in the SNN graph construction)
139 were inspected using a clustering tree drawn using *clustree* (v. 0.4.3 (Zappia and Oshlack,
140 2018)). Clusterings with 10 and 15 neighbours were further explored, as they yielded
141 numbers of clusters similar to the ones in the original publication. For both 10 and 15
142 neighbours, cluster separation was evaluated using three methods: approximate silhouette
143 width, neighborhood purity and pairwise modularity, as implemented in the *bluster* package
144 (v. 1.0.0 (Lun, 2020b)) in the *approxSilhouette*, *neighborPurity* and *pairwiseModularity*
145 functions. The 15 neighbour clustering showed slightly better separation so it was considered
146 for downstream analyses. In order to reconstruct the original cell type identities as identified

147 by the authors, the *AUCell* package (v. 1.12.0, (Aibar et al., 2017)) was used in conjunction
148 with the cluster marker genes as published by the authors, although these marker genes were
149 identified in the 10X dataset. Raw counts were ranked in each cell and the AUC for each
150 marker set was calculated; each cell was assigned the identity yielding the highest AUC value
151 using the 30% top ranking genes. AUCell is agnostic to the transcriptional space and to other
152 intrinsic properties of the dataset, which will be influenced by differences in filtering and
153 processing steps. Therefore the performance of AUCell was evaluated in this dataset
154 calculating the approximate silhouette width of the cell type assignment, and it was compared
155 to our clustering results by calculating pairwise Jaccard indices. Most identities (Hb1, Hb2,
156 Hb5, Hb6, Hb9, Hb1, Hb14, Hb15 and olfactory neurons) are reasonably well separated, but
157 only 4 (olfactory, Hb06, Hb03, and Hb08), are reproduced in our clustering with a Jaccard
158 index above 0.5 with any single cluster. This is in line with what the authors of the original
159 paper state regarding the poor performance of SmartSeq2 in terms of cell type recovery, and
160 is also to be expected when using cell type markers identified in the 10X dataset.
161
162 For the 10X datasets (larval) no filtering was performed as the distribution of QC metrics was
163 well within standard ranges, suggesting data were already filtered. Normalization, HVG
164 estimation and dimensionality reduction were performed in the same way as described above,
165 with the exception that there was no batch effect to account for and correct. An additional
166 doublet detection step was included using the *scDblFinder* package (v. 1.4.0, PMID
167 (Germain et al., 2020)), which flagged 172 barcodes as doublets and 4193 as singlets.
168 Doublets were not removed at this stage of the analysis. The intrinsic dimension estimation (k
169 = 66) yielded 12 dimensions to perform SNN graph clustering, which was performed using 5,
170 10, 15, 20, and 30 neighbours. In parallel, 36 dimensions were also considered as done by the
171 authors of the original publication. For the 12-dimensional space, 5 and 10 neighbours were
172 considered as they yielded numbers of clusters similar to those reported in the publication;
173 for the 36-dimensional space, 10 and 15 neighbours were considered. However, in both 12
174 and 36 dimensions a cluster was entirely made up of doublets, so doublets were removed and
175 the whole process (normalization, HVG selection and dimensionality reduction) was
176 repeated. Cluster separation metrics (approximate Silhouette and modularity) favoured
177 clustering with 10 neighbours (12 dimension) and 15 neighbours (36 dimensions). To
178 reproduce the original clustering results the AUCell package was used, and Jaccard indices
179 were used to match clusters to labels. In order to improve the label assignment, cells whose

180 top AUC label showed less than a 20% difference from the second best label were classified
181 as "ambiguous". Ambiguous labels were then reassigned using the closest centroid in the
182 approximate silhouette width calculation, thus making the labels conform more to the
183 transcriptional space. Improvements in the reassignment of these labels were measured by
184 comparing silhouette widths and the distribution maximum Jaccard indices for every cluster-
185 AUC label pair before and after reassignment. Both metrics showed an improvement in both
186 silhouette width and median best Jaccard index upon reassignment.
187
188 Adult zebrafish data was processed in the same above, accounting for batch effects (2
189 different captures). SNN graph construction with 4 neighbours in 16 dimensions was chosen
190 following the same pipeline and reasoning used in the larval dataset. AUCell was used to
191 determine identities using the markers provided by the authors of the original publication,
192 and the reassignment procedure described above was used to correct ambiguous labels.

193 2.2 Transgenic lines

194 *TgBAC(gng8:GAL4)*^{c426} (Hong et al., 2013) orT^{s1011t} (Scott and Baier, 2009) was used to
195 drive expression in the habenula. Calcium imaging was performed using
196 *Tg(elavl3:GCaMP6f)*^{a12200} and *Tg(UAS:GCaMP6s)*^{sq205}. *Tg(UAS:EGFP-2A-Δclocka-*
197 *5×MYC)*^{sq215}, abbreviated here as *Tg(UAS:EGFP-Δclocka)* was generated by injection of
198 *pT2-UAS:EGFP-2A-Δclocka-5xMYC* using Tol2 mediated transgenesis. All experiments
199 were carried out under guidelines approved by the IACUC of Biopolis (181408) and NTU
200 (A19014). The minimal number of animals was used.

201 2.3 Two-photon Imaging

202 *2.3.1 Extended imaging*

203 Based on the methods described by (Leung et al., 2019), non-anesthetized and non-paralyzed
204 larvae were mounted in 2% low melting agarose (LMA), in a glass-bottom dish (Matek). The
205 dish was filled with E3 medium supplemented with 1% Hepes and bubbled continuously with
206 carboxygen (95% oxygen). Imaging was performed with a Nikon A1R MP system, attached
207 to an upright FN1 microscope using a 25x 1.0 NA water dipping objective. Resonant
208 scanning was performed with 2x averaging, and 20 focal planes were collected, spaced 5 µm
209 apart. Signal was detected with a GaAsP detector. A piezo drive (Mad City Labs) was used
210 for fast focusing during imaging. 21 stacks were collected, at an interval of 1 second,

211 followed by a delay of 1 hour. The maximum imaging duration was 29 hours. After imaging,
212 larvae were checked for blood flow. They were then released from the agarose. Only data
213 from fish with normal blood flow and active swimming upon release were used for analysis.
214
215 To obtain a measure of calcium levels in the whole habenula, fluorescence intensities were
216 summed at each time point using Fiji. The intensity at each hour was averaged and z-scores
217 were plotted as a function of *zeitgeber* time.

218 ### *2.3.2 Short duration imaging*

219 6-day-old *Tg(elavl3:H2B-GCaMP6s)* or *Et(-1.5hsp70l:Gal4-VP16)*^{s1011t}, *Tg(UAS:GCaMP6f)*
220 larvae were immobilized with mivacurium, mounted in 2% low melting temperature agarose
221 and imaged with the two-photon system described above, using resonant scanning at a single
222 plan. Frame size was 512x256 pixels and 2x averaging was used, leading to a frame rate of
223 14.5 Hz. Segmentation of cells expressing cytoplasmic GCaMP6f was performed manually in
224 Fiji, while segmentation of cells expressing nuclear GCaMP6s was performed automatically
225 with Suite2p (Stringer and Pachitariu, 2019). Z-scores were obtained for each cell in a
226 recording, and cells were clustered using K-means clustering in Python. The classification
227 was performed using maximum likelihood and leave-one-out cross-validation. Specifically, at
228 each iteration we removed one dataset from the group and constructed empirical cluster
229 distributions for both categories (ZT3 and ZT15) from the remaining datasets. The removed
230 dataset was then assigned to the category whose empirical distribution maximized its
231 likelihood. This process was repeated independently until all datasets were classified.

232 ## 2.4 Immunohistochemistry and imaging of EGFP-ΔCLK

233 The *Tg(gng8:GAL4,UAS:EGFP-Δclocka)* larvae at the age of 7 dpf were fixed in 4% PFA at
234 4ºC for ~22 h. For immunostaining of extracted brains, skin covering the brain was manually
235 removed and exposed brains were washed 3 times in PBST. Antigen retrieval was performed
236 by incubating the fish in 150 mM Tris-HCl (pH 9.0) for 5 min at room temperature in order
237 to equilibrate, and by subsequent heating of the samples at 70˚C for 15 min. Following
238 several washes and a blocking step, samples were incubated in the rabbit anti-GFP primary
239 antibody (Torrey Pines Biolabs Inc., #TP401), diluted 1:500, and the mouse anti-Myc
240 antibody (9E10; Santa Cruz Biotechnology), diluted 1:100, at 4ºC for a few days. The
241 secondary antibodies used were Alexa Fluor 488 goat anti-rabbit (ThermoFisher and Abcam),
242 diluted 1:1000, and Alexa Fluor 647 goat anti-mouse (ThermoFisher), diluted 1:500. The

243 immunostained brains were mounted in 2% LMA in PBS and imaged using a Zeiss LSM800
244 confocal microscope equipped with 40X 0.7 NA water immersion objective.

245 2.5 Screening and selection of *Tg(gng8:GAL4,UAS:EGFP-Δclocka)* fish

246 All of the *Tg(gng8:GAL4,UAS:EGFP-*Δ*clocka)* fish used in the following experiments were
247 first screened for GFP fluorescence at 3 dpf using a Olympus MVX10 stereo fluorescence
248 microscope. Since the expression of EGFP-ΔCLK in the habenula was mosaic, only
249 individuals with expression in the majority of habenula cells were selected and used for
250 further experiments as ΔCLK-positive fish. Individuals with zero expression as well as larvae
251 exhibiting a minimal number of randomly labelled cells (less than ~15 cells per habenula)
252 were used as the control siblings (Figure S1). Following the behavioural experiments, larvae
253 were immobilized in tricaine methanesulfonate (MS-222; final concentration of 0.01 mg/ml;
254 Sigma), mounted in 2% LMA in E3 medium and the habenula-specific expression of EGFP
255 was assessed using a Zeiss LSM800 confocal microscope and 40X water dipping objective.

256 2.6 Quantification of DA and 5-HT levels

257 Three-month old female ΔCLK fish and their control siblings were immobilized using iced
258 water and euthanized by decapitation at ZT3 and ZT15. Whole brains, excluding the
259 olfactory bulb, were extracted in the ice-cold Ringer's solution (116 mM NaCl, 2.9 mM KCl,
260 1.8 mM $CaCl_2$, 5.0 mM HEPES, pH 7.2), snap-frozen in liquid nitrogen and stored in -80˚C
261 until further analysis. Supernatant was collected as described previously (Chatterjee and
262 Gerlai, 2009). Quantification of dopamine (DA) and serotonin (5-HT) was carried out by
263 LC/MS using the following analytical standards: dopamine hydrochloride (D2960000:
264 Sigma-Aldrich), dopamine-1,1,2,2-$d_4$hydrochloride (73483: Sigma-Aldrich) and serotonin
265 (14927: Sigma-Aldrich). Three biological replicates (i.e. measurements of different samples)
266 were performed.

267 2.7 Behaviour assays

268 *2.7.1 Acoustic startle following exposure to Schreckstoff*

269 Thirteen to sixteen day-old ΔCLK larvae and their non-expressing siblings were placed in
270 two transparent plastic tanks with dimensions of 80 x 54 x 33 (L x W x H in mm) and their
271 locomotor activity was recorded from above at 10 fps using a camera (acA2040-90µm USB
272 3.0; Basler). Each of the two tanks was filled with 20 mL of facility water and held 8 fish at

273 most. The water level in each tank was 5 mm in height to minimize vertical movement. The
274 alarm substance was freshly prepared from adult zebrafish each week (Mathuru et al., 2012),
275 and was tested for effectiveness on adults before use on larvae. An Arduino Grove Vibration
276 Motor was positioned in between the two plastic tanks, on the stage holding the tanks, to
277 provide the stimulus. The vibration was 1 sec in duration and was presented 3 times, at 1
278 minute intervals, starting five minutes before and after the delivery of the *Schreckstoff*. A
279 startle response was defined as a change in body orientation of more than 90 degrees within 5
280 sec in response to each vibration tone. The response (yes or no for each fish) was averaged
281 across 3 tones for each group to obtain a response percentage before and after the delivery of
282 the *Schreckstoff*. Both the vibration tones and the delivery of *Schreckstoff* were controlled by
283 an Arduino board synched with the video-recording Python codes. Experiments were
284 performed on 3 separate batches of larvae. A different batch of freshly prepared skin extract
285 was used for each experiment; the extract was verified for effectiveness by testing on adult
286 fish. Only extract that evoked freezing was used.
287

288 ### *2.7.2 Locomotor activity*

289 The *Tg(gng8:GAL4,UAS:EGFP-Δclocka)* larvae were raised under standard conditions. Each
290 experimental run involved animals from the same batch, originating from one pair of parents.
291 The larvae were screened and selected as described in the previous section. At the age of 6
292 dpf the larvae were placed individually in a 24-well plate filled with 1.5 ml of tank water per
293 well. The plate was then transferred into an incubator equipped with an IR camera (acA2040-
294 90µm USB 3.0: Basler), a white LED box and four IR LED bars (LBS2-00-080-3-IR850-
295 24V, 850 nm: TMS Lite). The camera and the LEDs were connected to a PC via a
296 microcontroller board (Arduino UNO SMD). At the onset of recording (ZT6 – 9), fish were
297 kept under ambient light, which was switched off at ZT14 and was kept off during the next
298 day for the monitoring of activity under DD. A customized script written in Python 2.7,
299 incorporating functions from the OpenCV library was used to control the Arduino
300 microcontroller and simultaneously video-track fish locomotor activity. The video was
301 captured using 576 x 864-pixel resolution at 10 frames per second and the background
302 subtraction method was implemented to extract the 'x' and 'y' coordinates of each fish
303 online. The position data was then converted to total distance (mm) travelled by each fish per
304 1 min time. The data conversion, further analysis and plotting were carried out using custom-
305 written Excel macros, Python 2.7 and Estimation Statistics (Ho et al., 2019).

306 ### *2.7.3 Arousal threshold*

307 Six days-old ΔCLK larvae and their control siblings were randomly placed in a 24-well plate
308 and their locomotor activity was video-tracked as described in the previous section. In order
309 to assess the arousal during sleep, vibration stimuli were applied through a speaker
310 controlled, via an Arduino microcontroller board, by a modified version of the activity-
311 tracking code in Python 2.7. Starting at ZT17, eighteen stimuli of nine different intensities,
312 where 50% of computer audio output represented the highest intensity, were delivered for
313 200 ms (starting from 0%) in 12-16% increments every minute, first in a descending and then
314 ascending order. The time interval between stimuli was determined based on previous
315 findings that suggest a 30-second inter-stimulus gap is sufficient to avoid behavioural
316 habituation (Burgess and Granato, 2007). The protocol was repeated at the commencement of
317 every hour until ZT22, while the onset by ascending or descending order was altered each
318 time. In total, 12 replicates (i.e. technical replicates) of each stimulus intensity were
319 generated. A fish was scored as responding if it moved more than 7 pixels (~ 4 mm)
320 following the stimulus delivery and the average percentage of responding fish was calculated
321 for each of the stimulus intensities (Woods et al., 2014). The observed values were corrected
322 for variations in the baseline locomotor activity, by first calculating the background
323 probability of locomotion as a percentage of larvae which moved more than 7 pixels 5 s
324 before the application of each stimulus. The average of 108 measures of the background
325 probability of locomotion was then used to calculate the corrected probability of response at
326 each of the stimulus intensities, implementing the following equation: corrected probability
327 of response = observed value x [(observed value - background offset) / (max observed value -
328 background offset)].

329 ### *2.7.4 Novel tank assay*

330 All experiments were conducted between ZT2 and ZT4 on 3-5 month-old adult zebrafish, as
331 described elsewhere (Haghani et al., 2019). Fish were recorded in pairs in a darkened room
332 with a black background, where tanks were illuminated from the top with a natural light LED
333 bar. Novel tanks were made of glass measuring 20 cm (L) by 5 cm (W) by 12 cm (H) with
334 opaque sides (to prevent fish from viewing each other), placed side by side. Fresh water from
335 the facility was added to tanks up to the 10 mL mark to make a total volume of 1 L. The
336 setup was placed within a curtained area to obscure the experimenter.
337

338 Prior to exposure to the novel tank, fish were handled carefully to ensure that handling stress
339 was minimized. Fish were gently netted in pairs from their home tanks in the facility to
340 smaller crossing tanks, where they were brought into the room with the behavioural setup.
341 Then, fish were netted into 100 mL beakers with ~30 mL of fish facility water and quickly
342 poured into the novel tank. The recording was started within 30 s of fish being in the
343 recording tanks. For exposure to *Schreckstoff,* fish were placed in 100 mL beakers containing
344 200 µL of heated skin extract (Chia et al., 2019) in 50 mL fish facility water for 2 minutes.
345 Fish were netted into another beaker containing fresh facility water before being poured into
346 the novel tank. Videos were acquired at 10 frames per second for 600 s (10 mins) using a
347 Basler Ace camera (acA1300–200 µm; 1,280 × 1,024). The position (x-y coordinates) of the
348 fish were tracked, and speed was binned by mm/s into a probability density curve.
349
350 For acute exposure to *Schreckstoff*, fish were first habituated in the glass tanks for 5-7 mins.
351 Then, fish were recorded in the tanks for 5 mins before 1 mL of 1:4 dilution of heated skin
352 extract was pipetted into the tanks. The recording continued for 5 mins after *Schreckstoff*
353 delivery for the alarm response to be observed. Two fish were tested at one time, each in a
354 separate tank, with one tank containing ΔCLK fish and the other a non-expressing sibling.
355 The tank used for a particular genotype was switched at every trial. Characteristic alarm
356 behaviours were quantified, such as time spent in the bottom third of the tank, number of
357 darting episodes (fish speed >5 SD above average swim speed for the first 5 mins), and
358 number of freezing episodes (movement of <5.5 mm per second). Tracking was automated to
359 prevent observer bias. Sample size was based on previous experiments (Chia et al., 2019).

360 ***2.7.5 Light/dark choice assay***

361 All experiments were performed between ZT2 and ZT9 in a behavioural arena within
362 blackout curtains as described previously (Cheng et al., 2016). Four transparent plastic tanks
363 (dimensions: 43 mm W × 60 mm L × 30 mm H) filled with 30 mL fresh tank water served as
364 assay chambers. Opaque cardboard sheets were placed between the 4 tanks. Tanks were
365 placed on an Apple iPad screen and videos (9 fps) were recorded on a USB3.0 Basler camera
366 (Model# acA2040-90umNIR 1440 × 1080 pixels) with a long-pass filter (MIDOPT, LP830
367 830 nm) placed above. Two IR light bars (850 nm peak from TMS-lite) positioned next to the
368 4 tanks served as an IR light source. The light/dark compartments were created by white and
369 black rectangles (with 50% transparency level for the black) on a Microsoft PowerPoint slide

370 displayed on the iPad Air at highest brightness level. Sample size was based on previous
371 experiments(Cheng et al., 2016).
372
373 Larvae were exposed either to *Schreckstoff* or to control water (embryo medium) in a
374 treatment tank of the same dimensions with the same volume of tank water for 10 minutes.
375 Larvae were then gently pipetted from the treatment tank into two wash-out tanks
376 sequentially before being placed into the dark/light test chamber. Real-time tracking of the
377 fish was achieved by custom-written Python codes using the OpenCV library and recorded as
378 coordinates of the centroid of the fish across time. Larval behaviour was recorded for 10
379 minutes. Offline analysis was performed using custom-written Excel macros to determine the
380 position of the animals, the number of entries into each compartment, the percentage of total
381 time spent in each compartment, etc. A few fish (N=2 in both the Control group and
382 Gng8/ΔCLK group) were excluded from the analysis because they were entirely immobile or
383 because of tracking errors.

384 2.8 In situ hybridization

385 Hybridisation chain reaction with split initiator probes was conducted using the HCR v3.0
386 protocol for whole-mount zebrafish embryos and larvae from Molecular Instruments. Probe
387 hybridization buffer, amplification buffer, probe wash buffer, probe sets and HCR amplifiers
388 were obtained from Molecular Instruments.
389
390 *Tg(gng8:GAL4, UAS:EGFP-Δclocka)* larvae were maintained at 28°C under the standard 14-
391 10h LD cycle. For characterization of clock genes under DD, nacre and *Tg(gng8:GAL4,*
392 *UAS:EGFP-Δclocka)* larvae were maintained under standard LD conditions transferred to a
393 dark room at ZT14 the day before fixation.
394
395 All *Tg(gng8:GAL4, UAS:EGFP-Δclocka)* larvae were screened for mosaic expression of
396 EGFP-ΔCLK at 5 dpf and EGFP-ΔCLK positive larvae were separated from non-expressing
397 siblings. All larvae were fixed at ZT3, ZT7, ZT11, ZT15, ZT19 and ZT23h with 4%
398 paraformaldehyde (PFA) in phosphate buffered saline (PBS) at 4°C in a 1.5mL eppendorf
399 tube (1 tube per time-point) and incubated at 4°C overnight. Fixations for DD larvae were
400 performed under dim light. For dehydration and permeabilization, larvae were washed 4 x 10
401 minutes and 1 x 50 minutes with 1mL of 100% methanol (MeOH) at room temperature, and

402 subsequently stored in -20°C for several days. For rehydration, larvae were washed 1 x 5
403 minutes with 1mL of 75% MeOH (in PBST), followed by 50%, and 25% MeOH (in PBST),
404 and subsequently 5 x 5 minutes washes with 100% PBST. Larvae were then treated with 1mL
405 of 30µg/mL proteinase K for 45 minutes at room temperature and washed twice with 1mL of
406 PBST without incubation. Postfixation of larvae was conducted by adding 1mL of 4% PFA
407 for 20 minutes at room temperature. The larvae were then washed 1 x 1 hour and 4 x 5
408 minutes with 1mL of PBST. For pre-hybridization, 4 larvae from each sample were
409 transferred to a 1.5 mL eppendorf tube and 500 µL of probe hybridization buffer was added
410 and incubated at 37°C for 30 minutes. For detection of clock genes, probe hybridisation
411 buffer was aspirated from the samples and probe solution (2 µL each of 1 µM *arntl1b* and
412 *per3* qHCR probe sets or 3 µL of *cry1a* dHCR probe set in 500 µL of probe hybridisation
413 buffer at 37°C) was added and incubated at 37°C for ~22 hours. Samples were washed 4 x
414 15 minutes with 500 µL of probe wash buffer at 37°C, followed by 2 x 5 minutes washes
415 with 500 µL of 5X SSCT at room temperature for removal of excess probes. 5X SSCT was
416 aspirated from the samples and 500 µL of amplification buffer was added and incubated for
417 30 minutes at room temperature. For amplification of signal, amplification buffer was
418 aspirated from the samples and hairpin solution (10 µL each of snap-cooled HCR amplifier
419 hairpins h1 and h2 for all 4 probe sets in 500 µL of amplification buffer at room temperature)
420 was added and incubated in a dark box at room temperature for ~22 hours. Hairpin solution
421 was then removed by 2 x 5 minutes and 2 x 30 minutes washes and another 1 x 5 minutes
422 wash with 500µL of 5X SSCT at room temperature. Samples were lastly stored at 4°C in a
423 dark box before microscopy.

424 ### *2.8.1 qHCR Imaging*

425 4 larvae from each sample were mounted in 2% LMA in PBS in dorsal view and imaged
426 using a Zeiss LSM800 upright confocal microscope with 40 x water dipping objective at 0.5x
427 zoom. The acquisition settings were identical in all experiments. Z-stacks were collected at
428 512x512 resolution, giving a x-y pixel size of 0.62 µm, and a z-step of 0.73 µm. Sample size
429 was based on (Trivedi et al., 2018).

430 ### *2.8.2 Image Analysis*

431 To quantify gene expression in the entire habenula across different fish, segmentation of
432 habenula was performed manually using the Segmentation Editor in Fiji (Schindelin et al.,
433 2012). The integrated intensity of *per3* and *arntl1b* was measured using the 3D Objects

434 Counter (Bolte and Cordelières, 2006). The ratio was calculated to compensate for potential
435 tube-tube variation as well as change in intensity with imaging depth. Values were plotted
436 using GraphPad Prism.
437
438 To compare the level of *per3* in ΔCLK expressing and non-expressing cells, within-fish
439 analysis was performed on single planes. ΔCLK cells were segmented by thresholding the
440 GFP signal, while the habenula was manually segmented. Masks for control cells were
441 obtained by subtracting the ΔCLK mask from the habenula mask. ROIs were then created,
442 and mean intensity measured, based on methods described by (Choi et al., 2018), i.e. with a
443 mean filter of 3 and background correction. Statistical analysis was performed with
444 estimation statistics (Ho et al., 2019). 5000 reshuffles of the control and test labels were
445 performed to calculate each permutation P value.

446 ***2.8.3 dHCR imaging***

447 Following label for *cry1a*, 3 larvae from each of 6 time-points were imaged with confocal
448 microscopy, using an Achroplan 63x water dipping objective and 2048 x 4093 image size,
449 giving a x-y pixel size of 0.0495 µm. z step was 0.78 µm. Sample size was based on Choi et
450 al, 2018. To analyse the images, the habenula in one plane ~ 10 µm from the surface was
451 manually segmented. Spots were identified in Fiji using a Laplacian transform with FeatureJ,
452 with the smoothing scale set at 5. The number of spots was counted using FindMaxima, with
453 the prominence > 10.0. Identical settings were used for acquisition and analysis of all dHCR
454 images.

455 # 3. Results

456 ## 3.1 Multiple clock genes are expressed in the zebrafish habenula

457 Using in situ hybridization in brain sections with DIG-labelled probes, a number of clock
458 genes, such as *per1b* and *bmal* (*arntl1a*), have been shown to be expressed in the habenula of
459 adult zebrafish (Weger et al., 2013). To better characterize clock gene expression in this
460 structure, we analyzed single cell transcriptomes of the zebrafish habenula (Pandey et al.,
461 2018). A diversity of clock gene components, including *arntl1b*, *arntl2*, *per1a*, *per2*, *per3*,
462 *cry1a*, *cry1ab*, *cry1ba*, *cry1bb*, *clocka*, *clockb* and *nr1d1* were found (Figure 1). These
463 transcripts were isolated from *gng8*-expressing habenula neurons, which are found

464 throughout the habenula (Hong et al., 2013; Pandey et al., 2018). All clusters contained clock
465 genes, suggesting that the molecular clock is broadly distributed.
466
467 To examine the temporal dynamics of the clock in larval zebrafish, quantitative in situ
468 hybridization using hybridization chain reaction (HCR) (Choi et al., 2018) was carried out
469 on fish that were fixed at 6 different time points (Figure 2). With qHCR imaging, *arntl1b*
470 appeared to be expressed at a higher level in the habenula compared to the rest of the brain
471 (Figure 2A), with a stronger signal at approximately *zeitgeber* time ZT 15; expression at ZT
472 19 and ZT 23 was detected at the posterior margins. *per3* was detectable broadly in the brain,
473 including the entire habenula, with strongest expression at ZT 23 and ZT 3 (Figure 2B).
474 Signal intensity obtained with qHCR imaging provides a relative measure of transcript level
475 (Choi et al., 2018), and can vary with sample thickness and between tubes. To minimize error
476 from these potential confounds, we calculated the ratio of *arntl1b/per3* as a means of
477 comparing gene expression between animals. This ratio showed a circadian variation, with a
478 peak at ZT 11 - 15 (Figure 2D). To test whether clock gene cycling requires light, we
479 examined expression in fish grown in constant darkness. The ratio of *arntl1b*/*per3* expression
480 was maximal at CT 15 and minimal at CT3 (Figure 2E-G). We used single molecule imaging,
481 with dHCR imaging of *cry1a*, to further test whether the clock is cycling. Again, a circadian
482 change in expression level was detected in the habenula in constant darkness (Fig 2H, I), with
483 a peak at CT3 and a trough at CT15, similar to what has been reported in other tissues under
484 LD (Cavallari et al., 2011) or DD conditions (Kobayashi et al., 2000). These observations
485 confirm previous findings using clock reporters (Wang et al., 2020; Weger et al., 2013) that
486 the molecular clock is active in the zebrafish habenula.

487 3.2 The zebrafish habenula displays circadian variation in intracellular calcium

488 The presence of the molecular clock should lead to a number of circadian changes in a cell.
489 One such change is the level of cytoplasmic calcium (Pennartz et al., 2002). To examine
490 intracellular calcium levels in the zebrafish habenula, two-photon imaging was carried out in
491 fish held in constant darkness. Confocal microscopy was not used to avoid light-induced
492 disruption of the molecular clock by visible light (Tamai et al., 2007). By imaging a series of
493 z-stacks every hour, such that the entire habenula could be captured (Figure 3A-D), we
494 observed an increase in overall fluorescence intensity during the subjective day, followed by
495 a decrease during the subjective night (Figure 3E; 5 out of 6 fish imaged). This finding is

496 consistent with the hypothesis that the habenula contains an active circadian clock that has
497 the potential to drive changes in the intracellular calcium even in the absence of light, a
498 prominent circadian *zeitgeber*.
499
500 In the mouse, neurons in both medial (Sakhi et al., 2014a) and lateral (Sakhi et al., 2014b)
501 habenula display spontaneous neural activity that varies across a circadian cycle. To assess
502 whether this is also the case in the zebrafish habenula, we carried out calcium imaging at ~15
503 Hz at a single plane. We imaged at two different time points, starting at ZT3 and ZT15. The
504 z-score for fluorescence of each cell was calculated, and a vector was generated for the
505 activity of cells with high variance. A difference was observed between the means of this
506 vector at ZT3 and ZT15 (Figure 3F). To further characterize the activity, cells were classified
507 using K-means clustering. The cluster composition was distinct between day and night
508 (Figure 3G). To test the robustness of this apparent difference, we asked if a classifier could
509 correctly assign a random dataset to either ZT3 or ZT15. Indeed, 21 out of 26 datasets of the
510 cytoplasmic indicator and 10 out of 13 datasets with the nuclear indicator were correctly
511 assigned. These findings suggest that neural activity in zebrafish habenula is different at day
512 versus night.

513 3.3 Expression of a truncated *clock* gene in the habenula affects function

514 The expression of clock genes and the circadian change in intracellular calcium in the
515 habenula raises the possibility that an intrinsic clock influences habenula function. To test
516 this, we selectively expressed a truncated *clocka* gene (Dekens and Whitmore, 2008), referred
517 to as Δ*clocka*, in the habenula. This construct has been shown to act in a dominant manner to
518 inhibit the molecular clock in the zebrafish pineal (Livne et al., 2016). Δ*clocka* was expressed
519 in the habenula using the GAL4/UAS system with *TgBAC(gng8:GAL4)* (Hong et al., 2013)
520 as the driver. In addition to Δ*clocka*, the effector construct also included enhanced green
521 fluorescent protein (EGFP), which was separated from ΔClocka (ΔCLK) by a 2A peptide
522 linker, thus enabling the expression of two separate proteins. The presence of EGFP in the
523 habenula neurons of *Tg(gng8:GAL4, UAS:EGFP-*Δ*clocka)* fish (Figure 4A, B) indicates that
524 the construct is expressed appropriately and enables convenient identification of ΔCLK-
525 positive individuals (Livne et al., 2016). Labelling with an antibody against the Myc tag,
526 which is fused in frame at the C-terminus of ΔCLK, indicates that the truncated protein is
527 translated (Fig. 4C). Cells expressing ΔCLK would be expected to have a lower level of

528 Clock-regulated genes such as *per*, than non-expressing cells. To assess this, qHCR imaging
529 was performed on larvae with scattered expression of ΔCLK, and the level of *per3* in cells
530 with EGFP expression was compared with the ratio in non-expressing cells in the same
531 sample. As seen in Fig. 4D the level of *per3* differed between ΔCLK and control cells at all
532 time points, with a paired Cohen's D of 1.58 [95.0%CI 1.03, 4.22] at CT3, 0.525 [95.0%CI
533 0.337, 4.25] at CT7, -1.89 [95.0%CI -4.78, -0.734] at CT11, -1.57 [95.0%CI -3.38, -1.15] at
534 CT15, 0.872 [95.0%CI 0.636, 2.26] at CT19 and 0.637 [95.0%CI 0.536, 0.816] at CT23. This
535 suggests that expression of ΔCLK influences the molecular clock, although it does not
536 eliminate cycling.
537
538 Given the partial inhibition shown by gene expression analysis, we asked whether is any
539 evidence that expression of ΔCLK affects habenula function. The habenula regulates the
540 broad release of serotonin and dopamine (Amo et al., 2010; Satar et al., 2020) and contains
541 cholinergic neurons (Hong et al., 2013). If expression of ΔCLK has any effect on habenula
542 function, the global levels of secreted serotonin, acetylcholine and dopamine, which vary in a
543 circadian fashion (Hut and Zee, 2011; Mendoza, 2017), should be affected. To test this,
544 brains were isolated from adult zebrafish expressing EGFP-ΔCLK and from their non-
545 expressing siblings, at ZT3 and ZT15. The supernatant from extracts were analysed by liquid
546 chromatography and mass spectrometry (LC/MS) (Chatterjee and Gerlai, 2009). While non-
547 expressing fish had a clear difference in the day- and night-time levels of dopamine (Figure
548 4E; mean difference = 124 pg/mg, $p < 0.0002$ by permutation t-test), there was almost no
549 difference in fish expressing ΔCLK protein (mean difference = 6.3 pg/mg, $p = 0.30$ by
550 permutation t-test). The mean difference in between day and night-time levels of serotonin
551 and acetylcholine levels was also higher in control fish (117 pg/mg and 454 pg/mg
552 respectively, $p < 0.0002$ by permutation t-test in both cases), compared to ΔCLK-positive fish
553 (68.1 pg/mg and 137 pg/mg respectively, $p < 0.0002$ by permutation t-test). This change of
554 neuromodulator levels is consistent with the notion that expression of ΔCLK in the habenula
555 affects function.

556 3.4 Habenula expression of ΔCLK reduces anxiety-like behaviour induced by 557 the alarm substance

558 We hypothesized that a stress response would be affected by the expression of ΔCLK in the
559 habenula. One such response for fish is the alarm response, which is triggered by the

560 pheromone *Schreckstoff*. In adult zebrafish, Schreckstoff causes an acute change in
561 swimming behaviour (Jesuthasan and Mathuru, 2008; Speedie and Gerlai, 2008). Following
562 transient exposure to *Schreckstoff*, fish display abnormal scototaxis (Maximino et al., 2014)
563 and heightened vigilance. To determine whether manipulation of the habenula clock
564 influenced the acute response, adult fish were placed individually in a test tank. After a
565 period of acclimatization, the alarm substance was introduced into the tank (Figure 5A).
566 Adult *Tg(gng8:GAL4, UAS:EGFP-Δclocka)* zebrafish showed an increase in darting (Figure
567 5C, paired mean difference of 1.33 seconds [95.0% CI 0.5, 2.67], p = 0.0260 Wilcoxon rank
568 sum test), as did their non-expressing siblings (paired mean difference of 1.25 seconds
569 [95.0% CI 0.417, 3.33], p = 0.0256 Wilcoxon rank sum test). There was no difference in the
570 movement to the tank base (Figure 5D; paired mean difference of 16.4 [95.0%CI 1.02, 41.2],
571 p = 0.530 for ΔCLK fish and 12.6 [95.0%CI -0.997, 28.1], p = 0.182 for siblings).
572
573 To monitor expectation of danger (or anxiety-like behaviour), individual fish were exposed to
574 the alarm substance in a beaker, then transferred to a novel tank containing fresh water
575 (Figure 5E). ΔCLK fish, in contrast to their non-expressing siblings, did not freeze, but
576 behaved similarly to fish that had been exposed to fish water (Figure 5F, G)). We also
577 monitored the post-exposure response of larval zebrafish, using a light-dark choice assay as
578 an indicator of stress (Steenbergen et al., 2011) (Figure 5H). Larval *Tg(gng8:GAL4,*
579 *UAS:EGFP-Δclocka)* fish displayed less dark avoidance after transient exposure to
580 Schreckstoff, as indicated by the increased amount of time spent in the dark side of the tank
581 (Figure 5I, J; mean difference of 0.0971 [95.0% CI 0.0475, 0.146], p = 0.001 permutation t-
582 test; Cohen's d = 1.16 [95% CI 0.481, 1.82]), in contrast to their non-expressing siblings
583 (mean difference of 0.0213 [95.0% CI -0.058, 0.0928], p = 0.588; Cohen's d = 0.224 [95%
584 CI -0.667, 10.8]). Together, these observations suggest that disruption of the habenula clock
585 leaves acute responses unaffected but reduces the expectation of danger that is evoked by
586 transient exposure to the alarm substance.
587
588 We next asked whether the expectation of danger induced by the alarm substance varies in a
589 circadian fashion in zebrafish; a circadian change has been noted in another species, *Rasbora*
590 *heteromorpha* (Thines and Vandenbussche, 1966). To do this, we exposed larval fish to the
591 alarm substance either at ZT3 or ZT15. Larval zebrafish respond to the alarm substance by
592 extended immobility (Jesuthasan et al., 2020). To sensitively detect this, a vibration was

593 presented five minutes before and after delivery of the alarm substance (Figure 6A). Control
594 zebrafish showed a reduction in startle after delivery of the alarm substance during the day
595 (ZT3, $p = 0.00248$, Pearson's chi-squared test in R), but not at night (ZT15, Figure 6B),
596 consistent with freezing during the day but not at night. *Tg(gng8:GAL4, UAS:EGFP-*
597 *Δclocka)* fish did not show a reduction in startle at day or at night (Figure 6C). These data
598 suggest that the extended freezing evoked by the alarm response is circadian in zebrafish and
599 is influenced by the habenula clock.

600 3.5 Expression of ΔCLK in the habenula does not affect pineal-regulated 601 circadian behaviour

602 We hypothesized that while the circadian clock in the habenula affects the response to a
603 stimulus that influences expectation, circadian behaviours that are under the control of the
604 pineal clock (Livne et al., 2016) should be unaffected. To test this, we analysed the rhythmic
605 locomotor activity of ΔCLK-positive larvae and their non-expressing siblings. All larvae
606 were entrained to the standard LD cycle and their locomotion was monitored for a few hours
607 during the light phase, followed by the onset of darkness at ZT14 for activity tracking during
608 the night. Subsequently, the fish were monitored for one day under constant darkness (DD),
609 in order to eliminate the masking effects of light and dark on clock-regulated behaviour
610 (Livne et al., 2016). As seen in Figure 7A-D, ΔCLK larvae showed a similar pattern of
611 locomotion as their non-expressing siblings, becoming mobile during the light phase and
612 during the subjective day, while exhibiting quiescent periods of inactivity during the 1st and
613 2nd night of the recording.
614
615 In addition to locomotion, we also examined arousal threshold, which is normally elevated
616 during the sleep-like state at night. Arousal threshold was measured by responsiveness to
617 auditory stimuli (Zhdanova et al., 2001). Nine different intensities were delivered between
618 ZT17 and ZT23, and a sudden change in locomotion was taken as an indicator of
619 responsiveness. A larva was scored as a responder if it moved more than 7 pixels after the
620 stimulus and the average percentage of responders was calculated for each stimulus intensity
621 per group for each experimental run ($N = 5$ experimental runs). Overall, no difference was
622 seen between ΔCLK larvae and their control siblings (Figure 7E, F). Together, these
623 experiments indicate that disruption of the habenula clock has relatively specific effects.

4. Discussion

Predictive coding has emerged in recent years as a highly effective paradigm for understanding how the brain functions (Clark, 2013; Friston, 2018). It was applied initially to sensory processing, including the visual system (Rao and Ballard, 1999), and has since been extended to include cognition and emotion (Barrett, 2017). This framework can also be used to understand psychiatric disorders such as depression and other stress-related disorders (Kaye and Krystal, 2020; Smith et al., 2021; Wilkinson et al., 2017). Given the broad relevance of predictive coding, a knowledge of the anatomical and physiological mechanisms underlying its implementation is of considerable interest. A key feature of predictive coding is the updating of expectations based on experience, and this involves the release of neuromodulators that indicate the sign and magnitude of error, as well as precision of prediction. The habenula is one regulator of these modulators, and the pattern of evoked activity and effects of manipulation are consistent with a role in predictive coding underlying motivated behaviour and response to stressors. Recent work has identified a number of mechanisms, such as regulation of membrane potential by astroglial cells (Cui et al., 2018), that influence habenula function by altering the level of spontaneous activity. Spontaneous activity determines the output of a network (Arieli et al., 1996) and is an important element of predictive coding (Hartmann et al., 2015). Here, we propose that the molecular clock, which influences spontaneous activity (Harvey et al., 2020), contributes to habenula function in predictive coding.

We have found that habenula clock in zebrafish is transcriptionally complex, consisting of multiple paralogs. Given the potential redundancy provided by this, we used expression of a truncated *clocka* gene (Dekens and Whitmore, 2008) to investigate the function of the habenula clock. This strategy is based on the discovery in mice that a truncated *clock* gene disrupts the circadian clock (Vitaterna et al., 1994), whereas a null mutant does not (DeBruyne et al., 2006). Expression of this antimorphic allele in the zebrafish pineal was previously shown to disruption in the expression of clock-regulated genes and in locomotion and sleep (Livne et al., 2016), indicating that it is an effective technique. Expression in the habenula appears to affect the molecular clock, as indicated by the change in *per3* gene expression. We did not observe a complete flattening of *per3* expression across the circadian cycle, however, indicating that inhibition is partial. While consistent with previous findings (Dekens and Whitmore, 2008), this level of inhibition appears sufficient to affect habenula

657 function, as indicated by change in day-night variation in neuromodulators that are under the
658 control of the habenula.
659
660 We observed that the freezing behaviour evoked by the alarm pheromone is lower at night
661 compared to the day, and this difference is reduced by expression of the truncated clock gene
662 specifically in the habenula. We also observed that dark avoidance induced by the alarm
663 substance is reduced by manipulation of the habenula clock. Thus, the data here are
664 consistent with the hypothesis that the habenula clock influences expectation of danger.
665 Clock gene expression has been reported in the habenula of other vertebrates, including mice
666 (Salaberry et al., 2019). A broad expression of a functional clock in the mammalian habenula
667 is consistent with electrical recordings obtained from slices, which show a change in firing
668 rate and resting membrane potential across the circadian cycle in both medial and lateral
669 habenula (Sakhi et al., 2014a, 2014b; Zhao and Rusak, 2005). The ability of an intrinsic clock
670 to influence habenula-dependent expectations may thus be conserved across vertebrates. This
671 represents a distinct mechanism from the role of clocks in other regions in the regulation of
672 stress (Koch et al., 2017). One implication of the findings here is that identifying clock-
673 regulated genes that regulate spontaneous activity in the habenula may be relevant in the
674 treatment of stress related disorders.

675 Acknowledgements

676 We thank Yoav Gothilf for providing the pT2-UAS:EGFP-2A-ΔCLK-5xMYC construct and
677 Marnie Halpern for providing the *TgBAC(gng8:GAL4)*^{c426} line. We also thank Hugh Piggins,
678 David Lyons, Caroline Wee and Ajay Mathuru for comments and discussion, and Erik
679 Meijering for FeatureJ. This work was funded by grants from the Singapore Ministry of
680 Education under its Academic Research Fund Tier 2 (MOE2017-T2-058) and the National
681 Research Foundation (NRF2017-NRF-ISF002-2676) to SJ, an ARAP fellowship from A*Star
682 to AB, and a Start-Up Grant from the Lee Kong Chian School of Medicine to SRL. The
683 funding agencies played no role in the study design or decision to publish.

684 Declaration of competing interests

685 The authors declare that no competing interests exist.

686 # Author contributions

687 AB, RKC, JCSM, GTJH and SJ performed experiments. AB, RKC, JCSM, S, GD, SL and SJ
688 analysed data. AB and SJ designed the study and wrote the manuscript.

689 # Figures

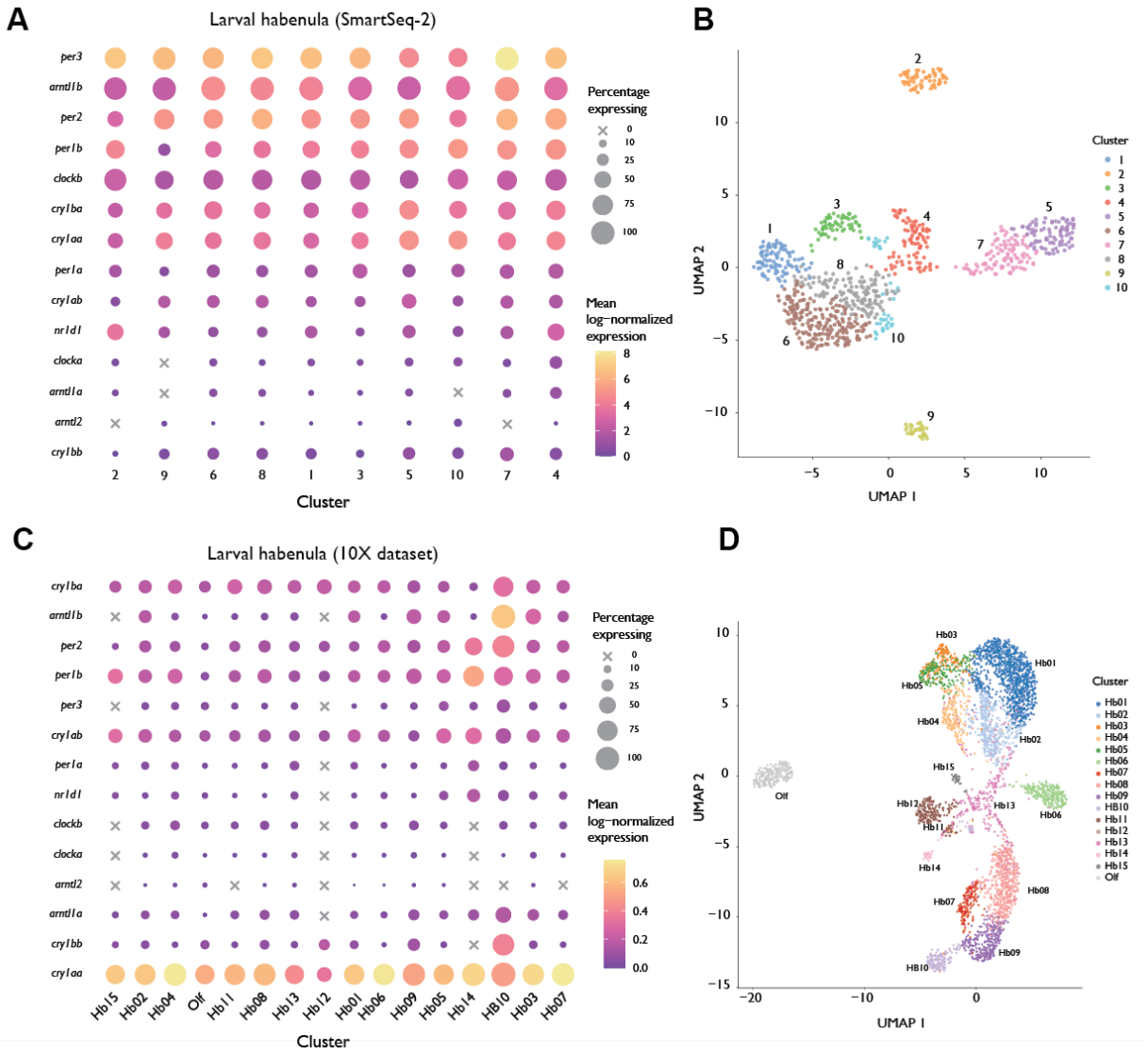

690
691

692 **Figure 1. Clock genes expression in the zebrafish habenula based on single cell RNA**
693 **sequencing**

694 **A)** Dot plot showing mean log-normalized expression per cluster and percentage of cells per
695 cluster expressing each gene in the SmartSeq-2 dataset from Pandey et al. **B)** t-SNE
696 representation of clustering results in the SmartSeq-2 dataset. Each point is a cell. **C)** same as

697 A) but in the 10X dataset. **D)** same as C but in the 10X dataset. The cluster assignment for the
698 10X dataset corresponds to those assigned by Pandey et al 2018.
699

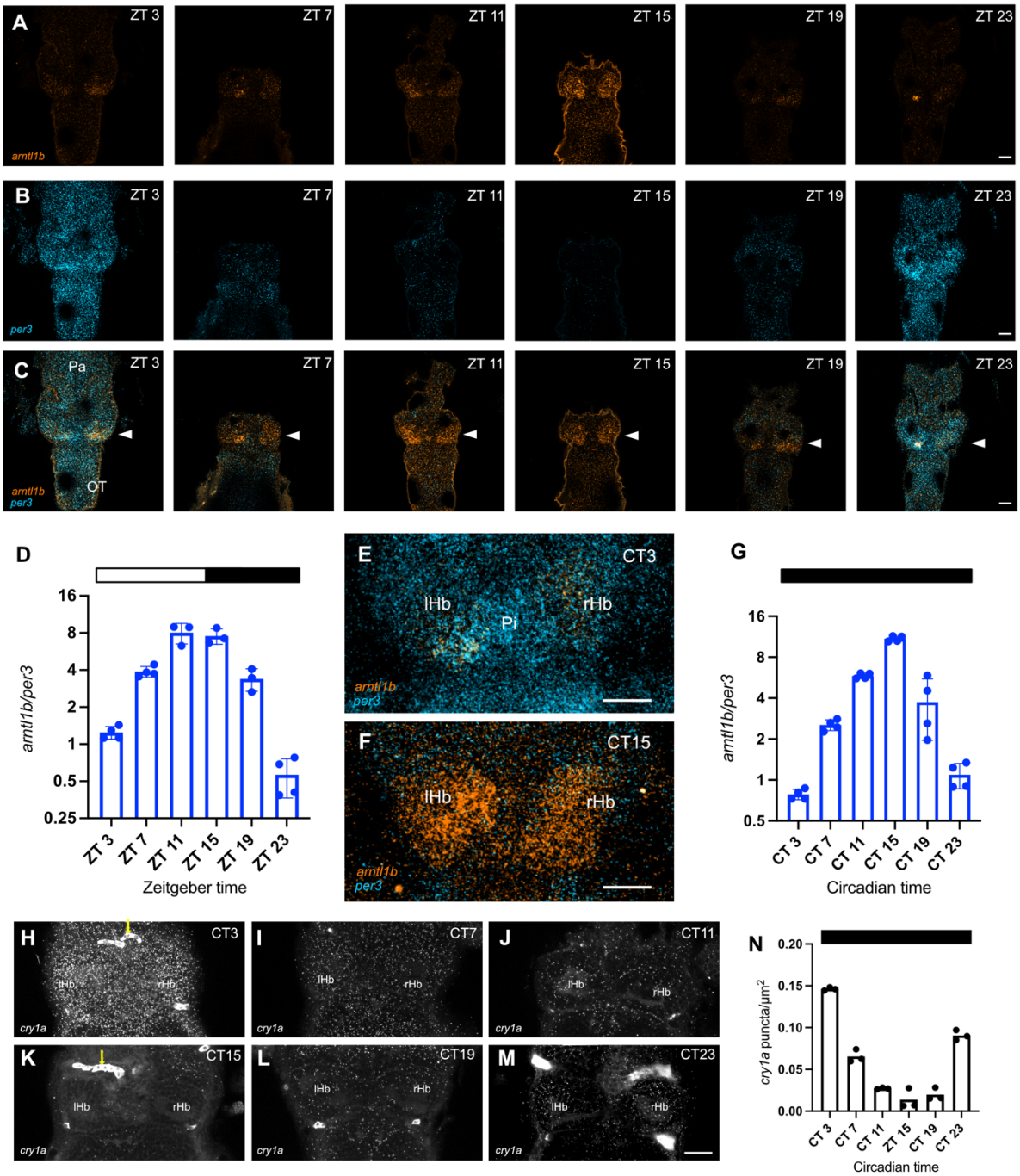

700
701 **Figure 2. Dynamics of clock gene expression in the zebrafish habenula. (A-C).** Single
702 optical sections of the brain of 6 day old larvae fixed at six different time points, labelled for
703 *arltn1b* (A) and *per3* (A) using hybridization chain reaction. **(C)** Merge of (A) and (B).
704 Arrowheads indicate the habenula. (**D**) Ratio of *arntl1b/per3* in the habenula of fish in a
705 normal LD cycle. (**E-G**) Expression of *per3* and *arntl1b* in the habenula of fish grown under

706 DD conditions. (**H-M**) *cry1a* expression in the habenula of fish grown under DD conditions.
707 Images in E and F are maximum projections of the entire habenula. Images in panels H-M are
708 maximum projections spanning 5 µm. The arrowheads indicate autofluorescent blood cells.
709 A, B, C, E , F, H-M are dorsal views with anterior to the top. The dots in panels D, G and N
710 indicate values for individual fish. The horizontal bars indicate illumination conditions. lHb:
711 left habenula; rHb: right habenula; Pi: pineal; Pa: pallium; OT: optic tectum. Scale bar = 25
712 µm.

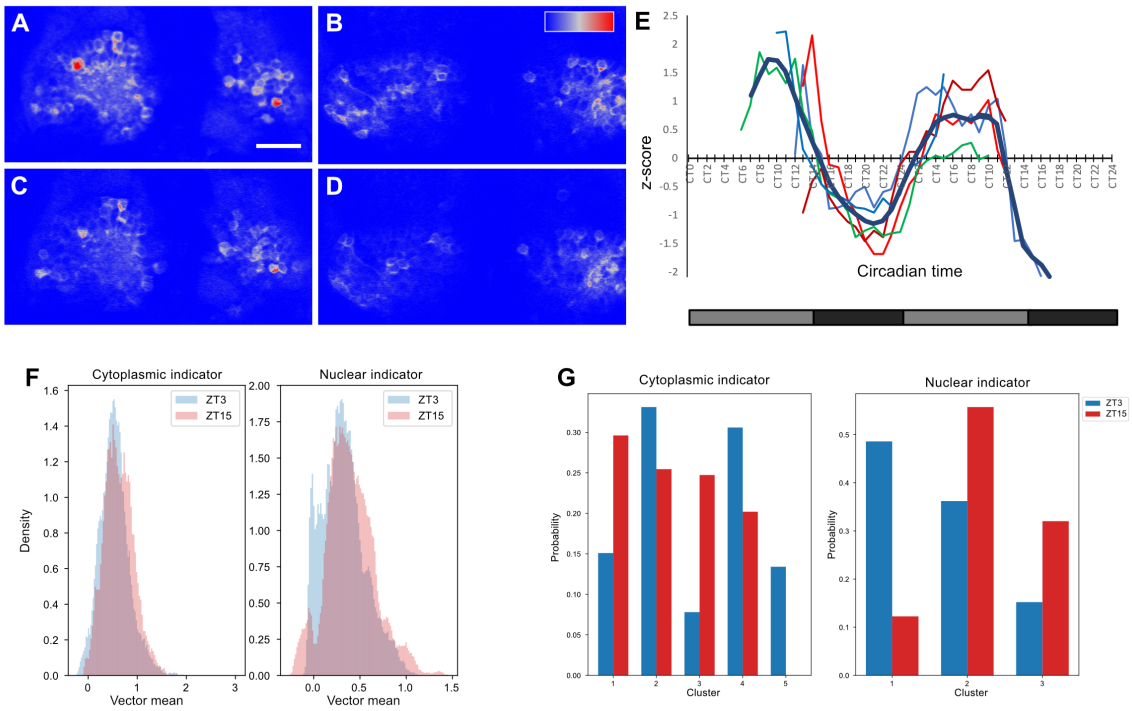

713

714 **Figure 3. Circadian variation in cytoplasmic calcium in habenula neurons.** (**A-E**) Long
715 duration multiplane recording of the habenula of *Et(GAL4s1011t),Tg(UAS:GCaMP6s)* larvae
716 in constant darkness. (A-D) Examples of imaging data from one fish at two different time
717 points, ZT5 (A, B) and ZT14 (C, D), and two different focal planes, dorsal (A, C) and ventral
718 (B, D). Scale bar = 25 µm, dorsal view with anterior to the top. (E) Average level of
719 cytoplasmic calcium in the habenula, as shown by intensity of GCaMP6s. Each coloured
720 trace represents one fish. The thicker black line is the mean. There is a reduction in
721 intracellular calcium levels during the subjective night. (F-G) Difference in relative activity
722 levels of habenula neurons between day (ZT3) and night (ZT15) as measured by both
723 cytoplasmic and nuclear GCaMP6s. (F) Distribution of the mean of vectors containing z-
724 scores of neurons with high variance in their activity. (G) K-means cluster distribution for the
725 same vectors.
726

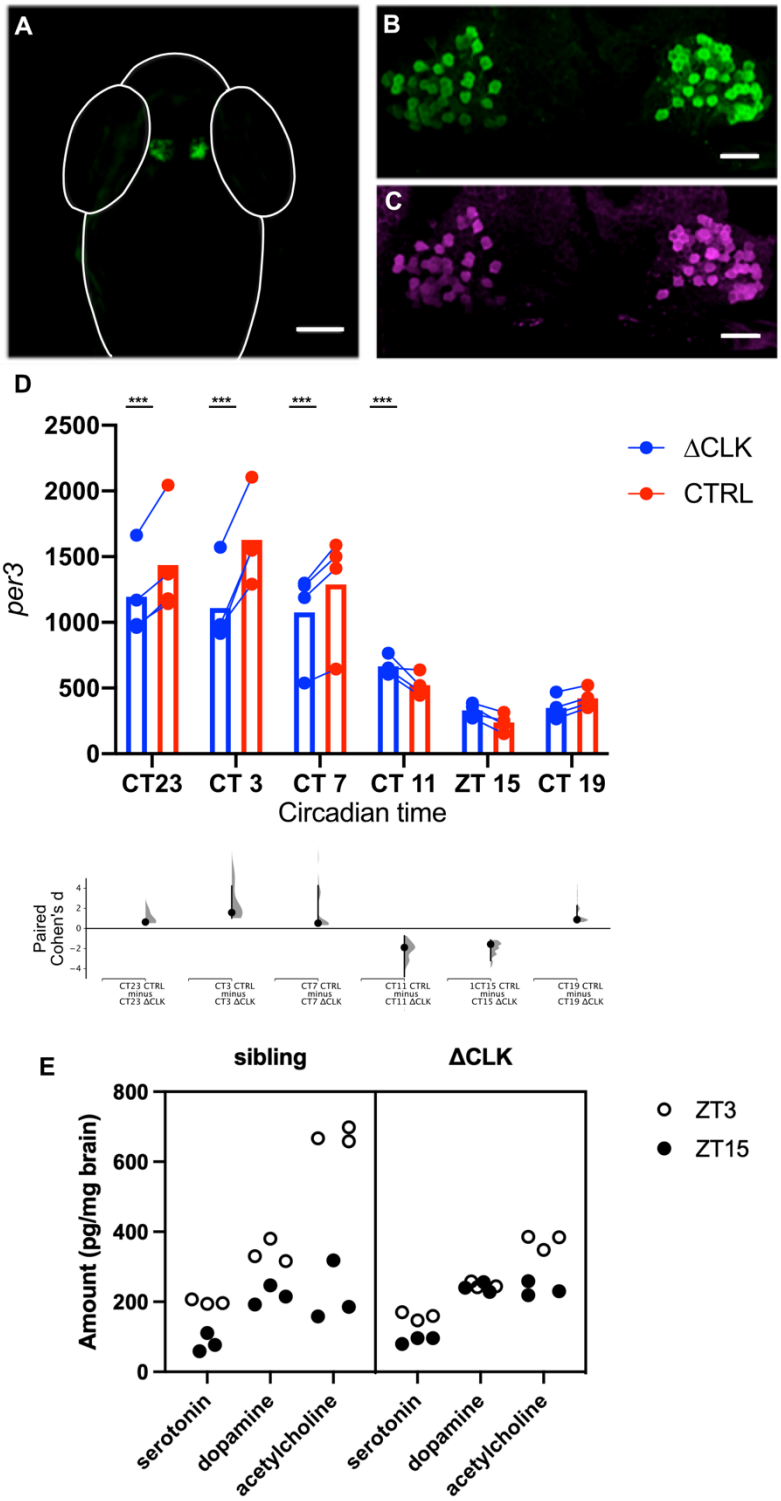

Figure 4. The effects of expressing truncated *clocka* in the habenula. (**A**) Specific expression of EGFP in the habenula of a *Tg(gng8:GAL4, UAS:EGFP-Δclocka)* fish. (**B**) At higher magnification, EGFP is visible in the cytoplasm of habenula neurons. (**C**) Detection of

734 Myc, which is fused to the C-terminus of ΔCLK, in the habenula of transgenic fish. **(D)** Level
735 of *per3* in the habenula of fish with mosaic expression of EGFP-ΔCLK, as determined by
736 qHCR imaging. The lower graph shows Cohen's d, indicating the degree of difference
737 between ΔCLK-expressing and non-expressing cells at each time point. Values are given in
738 the main text. **(E)** Effects of ΔCLK expression in the habenula on global neuromodulator
739 levels. Plot showing the amount of secreted serotonin, dopamine and acetylcholine in the
740 whole brain of and *Tg(gng8:GAL4, UAS:EGFP-Δclocka)* and sibling fish (N=3) at ZT3 and
741 ZT15. Fish with ΔCLK expression in the habenula have a reduced day-night change in levels.
742 Scale bar = 100 µm in panel A, 20 µm in panels B and C; *** indicates $p<0.0002$ by
743 permutation t-test.
744

745

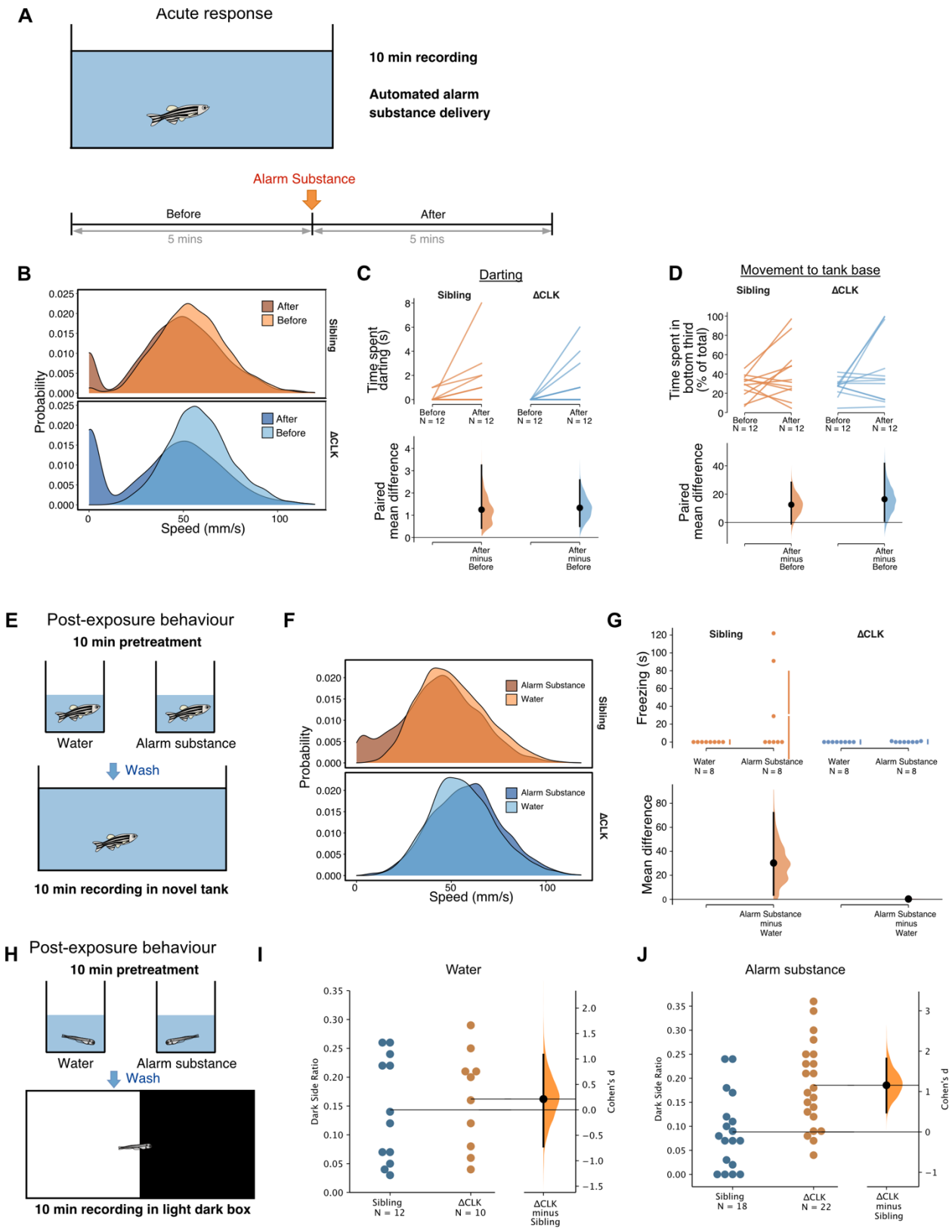

746

747 **Figure 5. The effects of the alarm substance *Schreckstoff* on *Tg(gng8:GAL4,***

748 ***UAS:EGFP-Δclocka)* fish**. (A-D) Acute effects in adult fish (N=12). (A) Schematic of the

749 experiment. (B) Speed distribution in fish before and after exposure to the alarm substance,

where the substance remained in the tank after delivery. (C-D) Time spent darting (C), restricted to the tank base (D) in the presence of the alarm substance. As indicated by the paired mean difference plots (lower plot), fish with and without expression of truncated *clocka* behave similarly. (E-G) Post-exposure behaviour in adult fish (N=8). (E) Schematic diagram of the experiment. (F) Speed distribution in a novel tank containing clean water, after exposure to alarm substance or clean water. (G) Only sibling fish exhibited freezing after exposure to alarm substance. (H-J) Post-exposure behaviour in 2 week-old zebrafish. (H) Schematic diagram of the experiment. (I) Percentage of time in the dark area of a tank, after 10 minutes of exposure to embryo water. (J) Percentage of time spent in the dark side after exposure to the alarm substance. *Tg(gng8:GAL4, UAS:EGFP-Δclocka)* fish spend more time in the dark side, with a Cohen's D of 1.2.

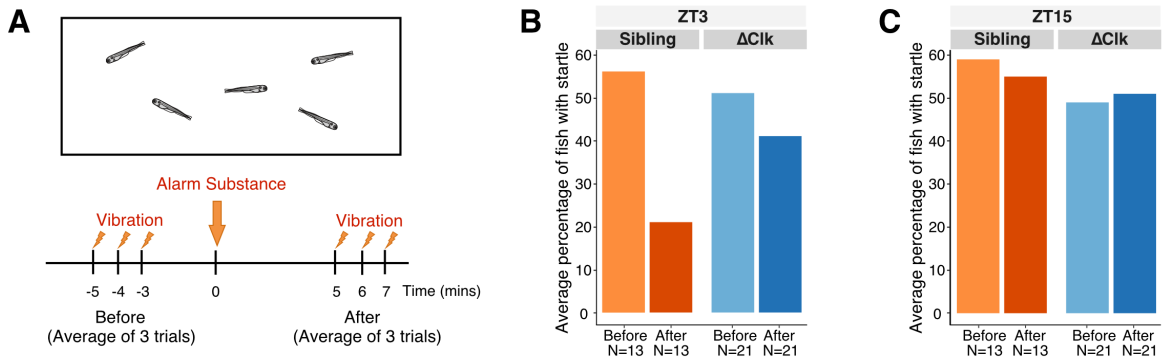

Figure 6. Day-night variation in the response of zebrafish to *Schreckstoff*. (A) Schematic of the experiment. To assess freezing in larval fish following exposure to the alarm substance, fish were exposed to vibrations in the day (ZT3) (B) or at night (ZT15) (C). Control fish, which are non-expressing siblings of *Tg(gng8:GAL4, UAS:Δclocka)* fish, show a reduction in startle after exposure during the day, but not at night. This response to alarm substance was not seen in *Tg(gng8:GAL4, UAS:Δclocka)* fish in the day or night.

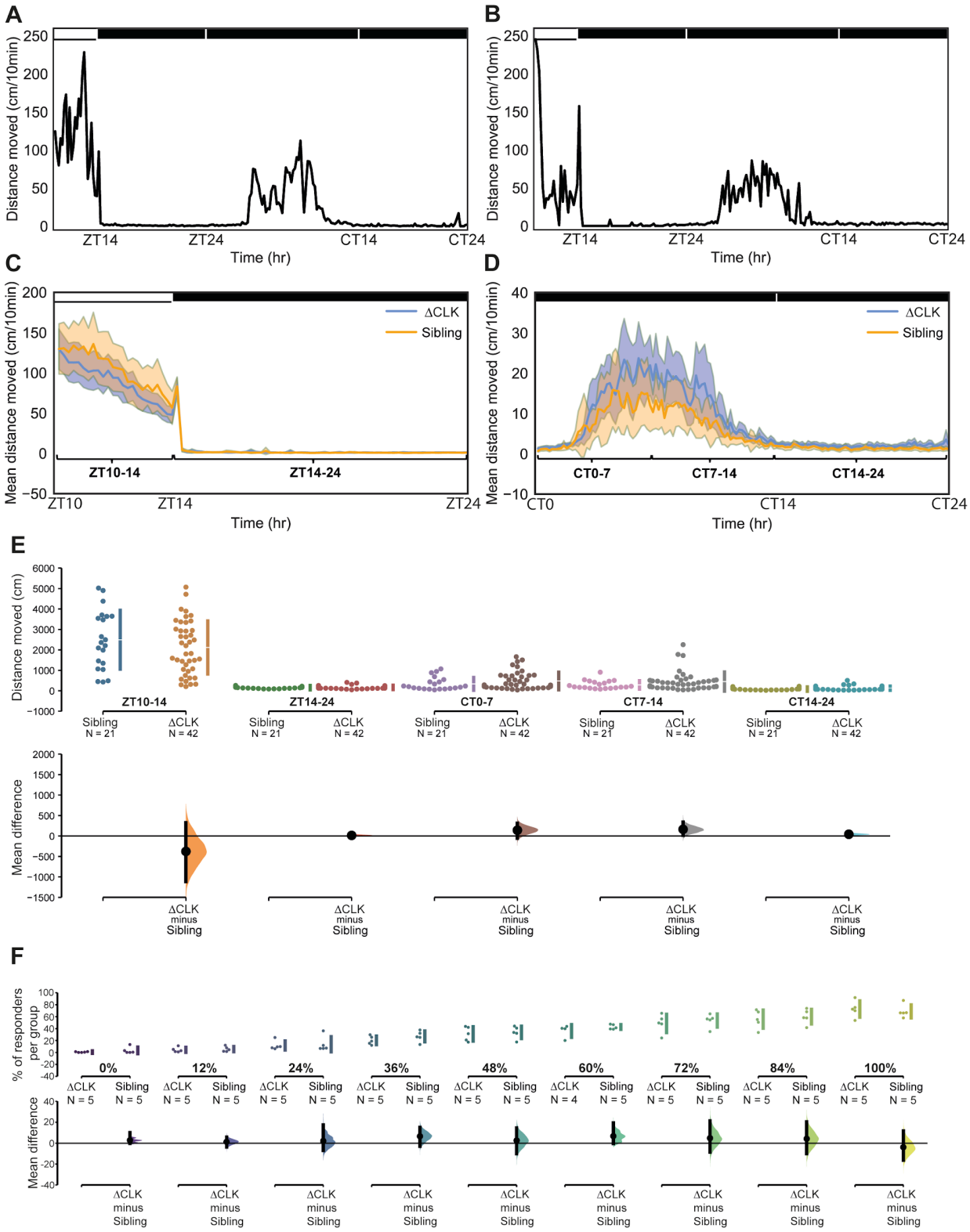

Figure 7. Sleep is unaltered in *Tg(gng8:GAL4, UAS:EGFP-Δclocka)* larvae

(**A, B**) Distances moved (cm/10min) by individual larvae from (A) Sibling group and (B) ΔCLK group are plotted against time (hr) over the time-course of the whole recording. CT =

774 circadian time. (**C, D**) Mean distances moved (cm/10min) of ΔCLK (blue) and Sibling
775 (orange) groups are plotted against time (hr) (C) during the first 14 hours of recording,
776 including 4 hours of light-phase and 10 hours in the dark during the night and (D) during the
777 subsequent 24 hours of recording under DD. 95% CIs are indicated by the shaded areas;
778 horizontal brackets indicate 5 analyzed timeframes. Black and white bars represent periods of
779 dark and light, respectively. (**E**) The Cumming estimation plot shows the mean differences in
780 5 timeframes of the recording: ZT10-14 (light-phase), ZT14-24 (1st night), CT0-7 (early
781 subjective day), CT7-14 (late subjective day) and CT14-24 (subjective night). The upper axis
782 shows the raw data, with each dot representing the overall distance moved (cm) by a single
783 larva; gapped vertical lines to the right of each group indicate mean ± SD. Each mean
784 difference is plotted on the lower axes as a bootstrap sampling distribution. Mean differences
785 are depicted as black dots and 95% CIs are indicated by the end of vertical error bars. (**F**)
786 Analysis of sensory responsiveness of the *Tg(gng8:GAL4, UAS:EGFP-*Δ*clocka)* larvae (7
787 dpf) during the delivery of auditory stimuli of 9 different intensities. The Cumming
788 estimation plot shows the mean differences for 9 comparisons, corresponding to 9 stimulus
789 intensities (0-100%). The raw data is plotted on the upper axis, each dot representing the
790 percentage of responders per single experimental run.
791

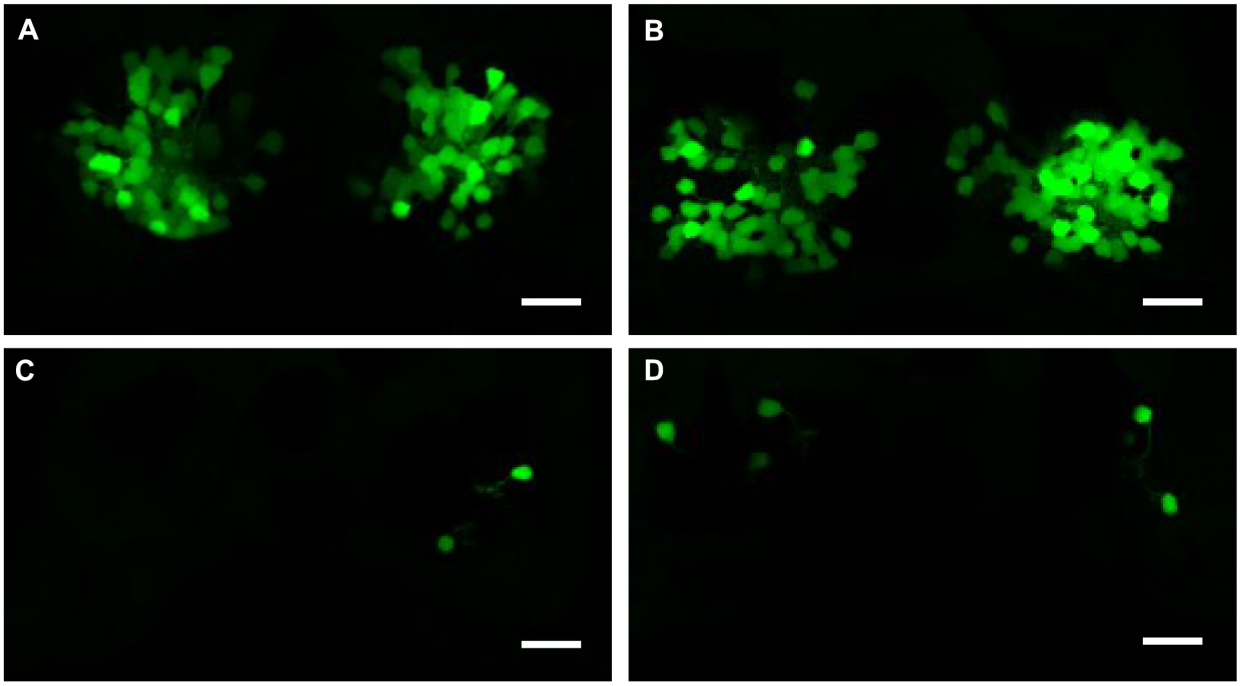

792

Figure S1. Examples of *Tg(gng8:GAL4, UAS:EGFP-Δclocka)* larval zebrafish with broad (A, B) and sparse (C, D) expression of EGFP in the habenula. All images are dorsal view, with anterior to the top. Scale bar = 10 μm.

References

Agetsuma, M., Aizawa, H., Aoki, T., Nakayama, R., Takahoko, M., Goto, M., Sassa, T., Amo, R., Shiraki, T., Kawakami, K., Hosoya, T., Higashijima, S., Okamoto, H., 2010. The habenula is crucial for experience-dependent modification of fear responses in zebrafish. Nature neuroscience 13, 1354–1356. https://doi.org/10.1038/nn.2654

Amezquita, R.A., Lun, A.T.L., Becht, E., Carey, V.J., Carpp, L.N., Geistlinger, L., Marini, F., Rue-Albrecht, K., Risso, D., Soneson, C., Waldron, L., Pagès, H., Smith, M.L., Huber, W., Morgan, M., Gottardo, R., Hicks, S.C., 2020. Orchestrating single-cell analysis with Bioconductor. Nat Methods 17, 137–145. https://doi.org/10.1038/s41592-019-0654-x

Amo, R., Aizawa, H., Takahoko, M., Kobayashi, M., Takahashi, R., Aoki, T., Okamoto, H., 2010. Identification of the zebrafish ventral habenula as a homolog of the mammalian lateral habenula. The Journal of neuroscience : the official journal of the Society for Neuroscience 30, 1566–1574. https://doi.org/10.1523/jneurosci.3690-09.2010

Amo, R., Fredes, F., Kinoshita, M., Aoki, R., Aizawa, H., Agetsuma, M., Aoki, T., Shiraki, T., Kakinuma, H., Matsuda, M., Yamazaki, M., Takahoko, M., Tsuboi, T., Higashijima, S., Miyasaka, N., Koide, T., Yabuki, Y., Yoshihara, Y., Fukai, T., Okamoto, H., 2014. The Habenulo-Raphe Serotonergic Circuit Encodes an Aversive Expectation Value Essential for Adaptive Active Avoidance of Danger. Neuron 84, 1034–1048. https://doi.org/10.1016/j.neuron.2014.10.035

Andalman, A.S., Burns, V.M., Lovett-Barron, M., Broxton, M., Poole, B., Yang, S.J., Grosenick, L., Lerner, T.N., Chen, R., Benster, T., Mourrain, P., Levoy, M., Rajan, K., Deisseroth, K., 2019. Neuronal Dynamics Regulating Brain and Behavioral State Transitions. Cell 177, 970-985.e20. https://doi.org/10.1016/j.cell.2019.02.037

Arieli, A., Sterkin, A., Grinvald, A., Aertsen, A., 1996. Dynamics of Ongoing Activity: Explanation of the Large Variability in Evoked Cortical Responses. Science 273, 1868–1871. https://doi.org/10.1126/science.273.5283.1868

Baño-Otálora, B., Piggins, H.D., 2017. Contributions of the lateral habenula to circadian timekeeping. Pharmacology, biochemistry, and behavior 162, 46–54. https://doi.org/10.1016/j.pbb.2017.06.007

Barrett, L.F., 2017. The theory of constructed emotion: an active inference account of interoception and categorization. Soc Cogn Affect Neur 12, 1–23. https://doi.org/10.1093/scan/nsw154

829 Berkes, P., Orbán, G., Lengyel, M., Fiser, J., 2011. Spontaneous Cortical Activity Reveals
830 Hallmarks of an Optimal Internal Model of the Environment. Science (New York, NY)
831 331, 83–87. https://doi.org/10.1126/science.1195870

832 Bolte, S., Cordelières, F.P., 2006. A guided tour into subcellular colocalization analysis in
833 light microscopy. J Microsc-oxford 224, 213–232.

834 Burgess, H.A., Granato, M., 2007. Modulation of locomotor activity in larval zebrafish
835 during light adaptation. The Journal of experimental biology 210, 2526–2539.
836 https://doi.org/10.1242/jeb.003939

837 Cavallari, N., Frigato, E., Vallone, D., Fröhlich, N., Lopez-Olmeda, J.F., Foà, A., Berti, R.,
838 Sánchez-Vázquez, F.J., Bertolucci, C., Foulkes, N.S., 2011. A Blind Circadian Clock in
839 Cavefish Reveals that Opsins Mediate Peripheral Clock Photoreception. Plos Biol 9,
840 e1001142. https://doi.org/10.1371/journal.pbio.1001142

841 Chatterjee, D., Gerlai, R., 2009. High precision liquid chromatography analysis of
842 dopaminergic and serotoninergic responses to acute alcohol exposure in zebrafish. Behav
843 Brain Res 200, 208–213.

844 Cheng, R.-K., Krishnan, S., Jesuthasan, S., 2016. Activation and inhibition of tph2
845 serotonergic neurons operate in tandem to influence larval zebrafish preference for light
846 over darkness. Sci Rep-uk 6, 20788. https://doi.org/10.1038/srep20788

847 Chia, J.S.M., Wall, E.S., Wee, C.L., Rowland, T.A.J., Cheng, R.-K., Cheow, K., Guillemin,
848 K., Jesuthasan, S., 2019. Bacteria evoke alarm behaviour in zebrafish. Nat Commun 10,
849 3831. https://doi.org/10.1038/s41467-019-11608-9

850 Choi, H.M.T., Schwarzkopf, M., Fornace, M.E., Acharya, A., Artavanis, G., Stegmaier, J.,
851 Cunha, A., Pierce, N.A., 2018. Third-generation in situ hybridization chain reaction:
852 multiplexed, quantitative, sensitive, versatile, robust. Development 145, dev165753.
853 https://doi.org/10.1242/dev.165753

854 Clark, A., 2013. Whatever next? Predictive brains, situated agents, and the future of cognitive
855 science. Behav Brain Sci 36, 181–204. https://doi.org/10.1017/s0140525x12000477

856 Csardi, G., Nepusz, T., 2006. The igraph software package for complex network research.
857 InterJournal Complex Systems, 1695.

858 Cui, Y., Yang, Y., Ni, Z., Dong, Y., Cai, G., Foncelle, A., Ma, S., Sang, K., Tang, S., Li, Y.,
859 Shen, Y., Berry, H., Wu, S., Hu, H., 2018. Astroglial Kir4.1 in the lateral habenula drives
860 neuronal bursts in depression. Nature 554, 323–327. https://doi.org/10.1038/nature25752

861 DeBruyne, J.P., Noton, E., Lambert, C.M., Maywood, E.S., Weaver, D.R., Reppert, S.M.,
862 2006. A Clock Shock: Mouse CLOCK Is Not Required for Circadian Oscillator Function.
863 Neuron 50, 465–477. https://doi.org/10.1016/j.neuron.2006.03.041

864 Dekens, M.P., Whitmore, D., 2008. Autonomous onset of the circadian clock in the zebrafish
865 embryo. The EMBO Journal 27, 2757–2765. https://doi.org/10.1038/emboj.2008.183

866 Delaunay, F., Thisse, C., Thisse, B., Laudet, V., 2003. Differential regulation of Period 2 and
867 Period 3 expression during development of the zebrafish circadian clock. Gene Expression
868 Patterns 3, 319–324. https://doi.org/10.1016/s1567-133x(03)00050-4

869 Friston, K., 2018. Does predictive coding have a future? Nat Neurosci 21, 1019–1021.
870 https://doi.org/10.1038/s41593-018-0200-7

871 Guilding, C., Hughes, A.T.L., Piggins, H.D., 2010. Circadian oscillators in the epithalamus.
872 Neuroscience 169, 1630–1639. https://doi.org/10.1016/j.neuroscience.2010.06.015

873 Haghani, S., Karia, M., Cheng, R.-K., Mathuru, A.S., 2019. An Automated Assay System to
874 Study Novel Tank Induced Anxiety. Front Behav Neurosci 13, 180.
875 https://doi.org/10.3389/fnbeh.2019.00180

876 Haghverdi, L., Lun, A.T.L., Morgan, M.D., Marioni, J.C., 2018. Batch effects in single-cell
877 RNA-sequencing data are corrected by matching mutual nearest neighbors. Nat
878 Biotechnol 36, 421–427. https://doi.org/10.1038/nbt.4091

879 Hartmann, C., Lazar, A., Nessler, B., Triesch, J., 2015. Where's the Noise? Key Features of
880 Spontaneous Activity and Neural Variability Arise through Learning in a Deterministic
881 Network. PLoS Computational Biology 11, e1004640.
882 https://doi.org/10.1371/journal.pcbi.1004640

883 Harvey, J.R.M., Plante, A.E., Meredith, A.L., 2020. Ion Channels Controlling Circadian
884 Rhythms in Suprachiasmatic Nucleus Excitability. Physiol Rev 100, 1415–1454.
885 https://doi.org/10.1152/physrev.00027.2019

886 Ho, J., Tumkaya, T., Aryal, S., Choi, H., Claridge-Chang, A., 2019. Moving beyond P
887 values: data analysis with estimation graphics. Nature methods 16, 565–566.
888 https://doi.org/10.1038/s41592-019-0470-3

889 Hong, E., Santhakumar, K., Akitake, C.A., Ahn, S.J., Thisse, C., Thisse, B., Wyart, C.,
890 Mangin, J.-M., Halpern, M.E., 2013. Cholinergic left-right asymmetry in the habenulo-
891 interpeduncular pathway. Proc National Acad Sci 110, 21171–21176.
892 https://doi.org/10.1073/pnas.1319566110

893 Hsu, Y.-W.A., Wang, S.D., Wang, S., Morton, G., Zariwala, H.A., Iglesia, H.O. de la,
894 Turner, E.E., 2014. Role of the dorsal medial habenula in the regulation of voluntary
895 activity, motor function, hedonic state, and primary reinforcement. The Journal of
896 neuroscience : the official journal of the Society for Neuroscience 34, 11366–11384.
897 https://doi.org/10.1523/jneurosci.1861-14.2014

898 Hut, R.A., Zee, E.A.V. der, 2011. The cholinergic system, circadian rhythmicity, and time
899 memory. Behav Brain Res 221, 466–480. https://doi.org/10.1016/j.bbr.2010.11.039

900 Jesuthasan, S., Krishnan, S., Cheng, R.-K., Mathuru, A., 2020. Neural correlates of state
901 transitions elicited by a chemosensory danger cue. Prog Neuro-psychopharmacology
902 Biological Psychiatry 110110. https://doi.org/10.1016/j.pnpbp.2020.110110

Jesuthasan, S.J., Mathuru, A.S., 2008. The alarm response in zebrafish: innate fear in a vertebrate genetic model. Journal of Neurogenetics 22, 211–228. https://doi.org/10.1080/01677060802298475

Jetti, S.K., Vendrell-Llopis, N., Yaksi, E., 2014. Spontaneous activity governs olfactory representations in spatially organized habenular microcircuits. Current biology : CB 24, 434–439. https://doi.org/10.1016/j.cub.2014.01.015

Johnsson, K., Soneson, C., Fontes, M., 2014. Low Bias Local Intrinsic Dimension Estimation from Expected Simplex Skewness. Ieee T Pattern Anal 37, 196–202. https://doi.org/10.1109/tpami.2014.2343220

Kaye, A.P., Krystal, J.H., 2020. Predictive Processing in Mental Illness: Hierarchical Circuitry for Perception and Trauma. J Abnorm Psychol 129, 629–632. https://doi.org/10.1037/abn0000628

Kim, U., Chang, S.-Y., 2005. Dendritic morphology, local circuitry, and intrinsic electrophysiology of neurons in the rat medial and lateral habenular nuclei of the epithalamus. The Journal of comparative neurology 483, 236–250. https://doi.org/10.1002/cne.20410

Kobayashi, Y., Ishikawa, T., Hirayama, J., Daiyasu, H., Kanai, S., Toh, H., Fukuda, I., Tsujimura, T., Terada, N., Kamei, Y., Yuba, S., Iwai, S., Todo, T., 2000. Molecular analysis of zebrafish photolyase/cryptochrome family: two types of cryptochromes present in zebrafish. Genes Cells 5, 725–738. https://doi.org/10.1046/j.1365-2443.2000.00364.x

Koch, C.E., Leinweber, B., Drengberg, B.C., Blaum, C., Oster, H., 2017. Interaction between circadian rhythms and stress. Neurobiology Stress 6, 57–67. https://doi.org/10.1016/j.ynstr.2016.09.001

Lee, A., Mathuru, A.S., Teh, C., Kibat, C., Korzh, V., Penney, T.B., Jesuthasan, S., 2010. The habenula prevents helpless behavior in larval zebrafish. Current biology 20, 2211–2216. https://doi.org/10.1016/j.cub.2010.11.025

Leung, L.C., Wang, G.X., Madelaine, R., Skariah, G., Kawakami, K., Deisseroth, K., Urban, A.E., Mourrain, P., 2019. Neural signatures of sleep in zebrafish. Nature 571, 198–204. https://doi.org/10.1038/s41586-019-1336-7

Livne, Z.B.-M., Alon, S., Vallone, D., Bayleyen, Y., Tovin, A., Shainer, I., Nisembaum, L.G., Aviram, I., Smadja-Storz, S., Fuentes, M., Falcón, J., Eisenberg, E., Klein, D.C., Burgess, H.A., Foulkes, N.S., Gothilf, Y., 2016. Genetically Blocking the Zebrafish Pineal Clock Affects Circadian Behavior. PLoS genetics 12, e1006445. https://doi.org/10.1371/journal.pgen.1006445

Lun, A., 2020a. BiocSingular: Singular Value Decomposition for Bioconductor Packages. R package version 1.6.0.

Lun, A., 2020b. bluster: Clustering Algorithms for Bioconductor.

940 Lun, A.T.L., McCarthy, D.J., Marioni, J.C., 2016. A step-by-step workflow for low-level
941 analysis of single-cell RNA-seq data with Bioconductor. F1000research 5, 2122.
942 https://doi.org/10.12688/f1000research.9501.2

943 Mathuru, A.S., Kibat, C., Cheong, W.F., Shui, G., Wenk, M.R., Friedrich, R.W., Jesuthasan,
944 S., 2012. Chondroitin Fragments Are Odorants that Trigger Fear Behavior in Fish. Current
945 biology : CB 22, 538–544. https://doi.org/10.1016/j.cub.2012.01.061

946 Matias, S., Lottem, E., Dugué, G.P., Mainen, Z.F., 2017. Activity patterns of serotonin
947 neurons underlying cognitive flexibility. Elife 6, e20552.
948 https://doi.org/10.7554/elife.20552

949 Matsumoto, M., Hikosaka, O., 2009. Representation of negative motivational value in the
950 primate lateral habenula. Nature neuroscience 12, 77–84. https://doi.org/10.1038/nn.2233

951 Maximino, C., Lima, M.G., Costa, C.C., Guedes, I.M.L., Herculano, A.M., 2014. Fluoxetine
952 and WAY 100,635 dissociate increases in scototaxis and analgesia induced by conspecific
953 alarm substance in zebrafish (Danio rerio Hamilton 1822). Pharmacology, biochemistry,
954 and behavior 124, 425–433. https://doi.org/10.1016/j.pbb.2014.07.003

955 McCarthy, D.J., Campbell, K.R., Lun, A.T.L., Wills, Q.F., 2017. Scater: pre-processing,
956 quality control, normalization and visualization of single-cell RNA-seq data in R.
957 Bioinformatics btw777. https://doi.org/10.1093/bioinformatics/btw777

958 Mendoza, J., 2017. Circadian neurons in the lateral habenula: Clocking motivated behaviors.
959 Pharmacology, biochemistry, and behavior 162, 55–61.
960 https://doi.org/10.1016/j.pbb.2017.06.013

961 Moran, R.J., Campo, P., Symmonds, M., Stephan, K.E., Dolan, R.J., Friston, K.J., 2013. Free
962 Energy, Precision and Learning: The Role of Cholinergic Neuromodulation. J Neurosci
963 33, 8227–8236. https://doi.org/10.1523/jneurosci.4255-12.2013

964 Pandey, S., Shekhar, K., Regev, A., Schier, A.F., 2018. Comprehensive Identification and
965 Spatial Mapping of Habenular Neuronal Types Using Single-Cell RNA-Seq. Current
966 biology : CB 28, 1052-1065.e7. https://doi.org/10.1016/j.cub.2018.02.040

967 Pennartz, C.M.A., Jeu, M.T.G. de, Bos, N.P.A., Schaap, J., Geurtsen, A.M.S., 2002. Diurnal
968 modulation of pacemaker potentials and calcium current in the mammalian circadian
969 clock. Nature 416, 286–290. https://doi.org/10.1038/nature728

970 Rao, R.P.N., Ballard, D.H., 1999. Predictive coding in the visual cortex: a functional
971 interpretation of some extra-classical receptive-field effects. Nat Neurosci 2, 79–87.
972 https://doi.org/10.1038/4580

973 Ren, J., Qin, C., Hu, F., Tan, J., Qiu, L., Zhao, S., Feng, G., Luo, M., 2011. Habenula
974 "cholinergic" neurons co-release glutamate and acetylcholine and activate postsynaptic
975 neurons via distinct transmission modes. Neuron 69, 445–452.
976 https://doi.org/10.1016/j.neuron.2010.12.038

977 Sakhi, K., Belle, M.D.C., Gossan, N., Delagrange, P., Piggins, H.D., 2014a. Daily variation
978 in the electrophysiological activity of mouse medial habenula neurones. The Journal of
979 Physiology 592, 587–603. https://doi.org/10.1113/jphysiol.2013.263319

980 Sakhi, K., Wegner, S., Belle, M.D.C., Howarth, M., Delagrange, P., Brown, T.M., Piggins,
981 H.D., 2014b. Intrinsic and extrinsic cues regulate the daily profile of mouse lateral
982 habenula neuronal activity. The Journal of physiology 592, 5025–5045.
983 https://doi.org/10.1113/jphysiol.2014.280065

984 Salaberry, N.L., Hamm, H., Felder-Schmittbuhl, M.-P., Mendoza, J., 2019. A
985 suprachiasmatic-independent circadian clock(s) in the habenula is affected by Per gene
986 mutations and housing light conditions in mice. Brain Struct Funct 224, 19–31.
987 https://doi.org/10.1007/s00429-018-1756-4

988 Satar, N.M.A., Ogawa, S., Parhar, I.S., 2020. Kisspeptin-1 regulates forebrain dopaminergic
989 neurons in the zebrafish. Sci Rep-uk 10, 19361. https://doi.org/10.1038/s41598-020-
990 75777-0

991 Schindelin, J., Arganda-Carreras, I., Frise, E., Kaynig, V., Longair, M., Pietzsch, T.,
992 Preibisch, S., Rueden, C., Saalfeld, S., Schmid, B., Tinevez, J.-Y., White, D.J.,
993 Hartenstein, V., Eliceiri, K., Tomancak, P., Cardona, A., 2012. Fiji: an open-source
994 platform for biological-image analysis. Nat Methods 9, 676–682.
995 https://doi.org/10.1038/nmeth.2019

996 Schultz, W., 1998. Predictive reward signal of dopamine neurons. Journal of
997 neurophysiology 80, 1–27.

998 Scott, E.K., Baier, H., 2009. The Cellular Architecture of the Larval Zebrafish Tectum, as
999 Revealed by Gal4 Enhancer Trap Lines. Front Neural Circuit 3, 13.
1000 https://doi.org/10.3389/neuro.04.013.2009

1001 Smith, R., Badcock, P., Friston, K.J., 2021. Recent advances in the application of predictive
1002 coding and active inference models within clinical neuroscience. Psychiat Clin Neuros 75,
1003 3–13. https://doi.org/10.1111/pcn.13138

1004 Speedie, N., Gerlai, R., 2008. Alarm substance induced behavioral responses in zebrafish
1005 (Danio rerio). Behav Brain Res 188, 168–177. https://doi.org/10.1016/j.bbr.2007.10.031

1006 Steenbergen, P.J., Richardson, M.K., Champagne, D.L., 2011. Patterns of avoidance
1007 behaviours in the light/dark preference test in young juvenile zebrafish: a pharmacological
1008 study. Behav Brain Res 222, 15–25. https://doi.org/10.1016/j.bbr.2011.03.025

1009 Stringer, C., Pachitariu, M., 2019. Computational processing of neural recordings from
1010 calcium imaging data. Curr Opin Neurobiol 55, 22–31.
1011 https://doi.org/10.1016/j.conb.2018.11.005

1012 Takahashi, J.S., 2017. Transcriptional architecture of the mammalian circadian clock. Nat
1013 Rev Genet 18, 164–179. https://doi.org/10.1038/nrg.2016.150

1014 Tamai, T.K., Young, L.C., Whitmore, D., 2007. Light signaling to the zebrafish circadian
1015 clock by Cryptochrome 1a. Proc National Acad Sci 104, 14712–14717.
1016 https://doi.org/10.1073/pnas.0704588104

1017 Thines, G., Vandenbussche, E., 1966. The effects of alarm substance on the schooling
1018 behaviour of rasbora heteromorpha Duncker in day and night conditions. Anim Behav 14,
1019 296–302. https://doi.org/10.1016/s0003-3472(66)80086-6

1020 Trivedi, V., Choi, H.M.T., Fraser, S.E., Pierce, N.A., 2018. Multidimensional quantitative
1021 analysis of mRNA expression within intact vertebrate embryos. Development 145,
1022 dev156869. https://doi.org/10.1242/dev.156869

1023 Vitaterna, M., King, D., Chang, A., Kornhauser, J., Lowrey, P., McDonald, J., Dove, W.,
1024 Pinto, L., Turek, F., Takahashi, J., 1994. Mutagenesis and mapping of a mouse gene,
1025 Clock, essential for circadian behavior. Science 264, 719–725.
1026 https://doi.org/10.1126/science.8171325

1027 Wang, H., Yang, Z., Li, X., Huang, D., Yu, S., He, J., Li, Y., Yan, J., 2020. Single-cell in
1028 vivo imaging of cellular circadian oscillators in zebrafish. Plos Biol 18, e3000435.
1029 https://doi.org/10.1371/journal.pbio.3000435

1030 Weger, M., Weger, B.D., Diotel, N., Rastegar, S., Hirota, T., Kay, S.A., Strähle, U.,
1031 Dickmeis, T., 2013. Real-time in vivo monitoring of circadian E-box enhancer activity: A
1032 robust and sensitive zebrafish reporter line for developmental, chemical and neural
1033 biology of the circadian clock. Developmental Biology 380, 259–273.
1034 https://doi.org/10.1016/j.ydbio.2013.04.035

1035 Wilkinson, S., Dodgson, G., Meares, K., 2017. Predictive Processing and the Varieties of
1036 Psychological Trauma. Front Psychol 08, 1840. https://doi.org/10.3389/fpsyg.2017.01840

1037 Woods, I.G., Schoppik, D., Shi, V.J., Zimmerman, S., Coleman, H.A., Greenwood, J., Soucy,
1038 E.R., Schier, A.F., 2014. Neuropeptidergic signaling partitions arousal behaviors in
1039 zebrafish. The Journal of neuroscience : the official journal of the Society for
1040 Neuroscience 34, 3142–3160. https://doi.org/10.1523/jneurosci.3529-13.2014

1041 Yang, Y., Cui, Y., Sang, K., Dong, Y., Ni, Z., Ma, S., Hu, H., 2018. Ketamine blocks
1042 bursting in the lateral habenula to rapidly relieve depression. Nature 554, 317–322.
1043 https://doi.org/10.1038/nature25509

1044 Zappia, L., Oshlack, A., 2018. Clustering trees: a visualisation for evaluating clusterings at
1045 multiple resolutions. Gigascience 7, giy083-. https://doi.org/10.1093/gigascience/giy083

1046 Zhao, H., Rusak, B., 2005. Circadian firing-rate rhythms and light responses of rat habenular
1047 nucleus neurons in vivo and in vitro. 132, 519–528.
1048 https://doi.org/10.1016/j.neuroscience.2005.01.012

1049 Zhdanova, I.V., Wang, S.Y., Leclair, O.U., Danilova, N.P., 2001. Melatonin promotes sleep-
1050 like state in zebrafish. Brain research 903, 263–268.

1051